Endocardial HDAC3 is required for myocardial trabeculation

Running title: HDAC3 is required for myocardial trabeculation

Jihyun Jang[1,2], Mette Bentsen[3], Ye-Jun Kim[4], Erick Kim[4], Vidu Garg[1,2], Chen-Leng Cai[5], Mario Looso[3], Deqiang Li[1, 2]

[1]Center for Cardiovascular Research, Abigail Wexner Research Institute, Nationwide Children's Hospital, Columbus, OH 43215, USA

[2]Department of Pediatrics, The Ohio State University College of Medicine, Columbus, OH 43215, USA

[3]Bioinformatics Core Unit (BCU), Max Planck Institute for Heart and Lung Research, 61231, Bad Nauheim, Germany

[4]Department of Surgery, University of Maryland School of Medicine, Baltimore, MD 21201, USA

[5]Department of Pediatrics, Herman Wells Center for Pediatric Research, Indiana University School of Medicine, Indianapolis, IN 46201, USA

Address correspondence to:

Deqiang Li, MD&PhD

575 Children's Drive, Room WB4329,

Columbus, OH 43215, USA

Phone: 614-355-5826

Email: Deqiang.Li@nationwidechildrens.org

Abstract

Background

Trabeculation, a key process in early heart development, is the formation of myocardial trabecular meshwork. The failure of trabeculation often leads to embryonic lethality. Support from endocardial cells, including the secretion of extracellular matrix (ECM) and growth factors is critical for trabeculation; however, it is unknown how the secretion of ECM and growth factors is initiated and regulated by endocardial cells.

Methods

Various cellular and mouse models in conjunction with biochemical and molecular tools were employed to study the role of histone deacetylase 3 (HDAC3) in the developing endocardium.

Results

We found that genetic deletion of *Hdac3* in endocardial cells in mice resulted in early embryo lethality presenting as a hypotrabeculation cardiac phenotype. Single cell RNA sequencing identified several ECM components including collagens that were significantly downregulated in *Hdac3* knockout (KO) endocardial cells. When cultured with supernatant from *Hdac3* KO mouse cardiac endothelial cells (MCECs), wild-type mouse embryonic cardiomyocytes showed decreased proliferation, suggesting that growth signaling from *Hdac3* KO MCECs is disrupted. Subsequent transcriptomic analysis revealed that transforming growth factor ß3 (TGFß3) was significantly downregulated in *Hdac3* KO MCECs and *Hdac3* cardiac endothelial KO hearts. Mechanistically, we identified that microRNA (miR)-129-5p was significantly upregulated in *Hdac3* KO MCECs and *Hdac3* cardiac endothelial KO hearts. Overexpression of miR-129-5p repressed

47 *Tgfß3* expression in wild-type MCECs, whereas knockdown of miR-129-5p restored
48 *Tgfß3* expression in *Hdac3* KO MCECs.

49 **Conclusion**

50 Our findings reveal a critical signaling pathway in which endocardial HDAC3 promotes
51 trabecular myocardium growth by stimulating TGFß signaling through repressing miR-
52 129-5p, providing novel insights into the etiology of congenital heart disease and
53 conceptual strategies to promote myocardial regeneration.

54

55

Key Words

Hdac3; epigenetics; endocardium; cardiomyocyte; heart development; trabeculation

Non-Standard Abbreviations and Acronyms

Hdac3, histone deacetylase 3

CEC, cardiac endothelial cell

MCEC. mouse cardiac endothelial cell

ECM, extracellular matrix

CM, cardiomyocyte

TGFß, transforming growth factor ß

miR, microRNA

GFP, green fluorescent protein

IHC, immunohistochemistry

GAPDH, Glyceraldehyde 3-phosphate Dehydrogenase

71 **Introduction**

72 Congenital heart disease (CHD) is the most common congenital disorder, and the leading
73 cause of mortality from birth defects[1]. Defective myocardial growth is either the primary
74 manifestation or associated with many forms of CHD[2, 3]. In the early primitive heart
75 (mouse embryonic day 8-10), inner cardiac endothelial cells (CECs), also called
76 endocardial cells, and outer cardiomyocytes (CMs), which are separated by extracellular
77 matrix (ECM), co-contribute to early myocardial trabeculation (i.e., formation of
78 myocardial meshwork extending to cardiac chamber)[4-6]. CECs juxtapose myocardial
79 trabeculae and lead myocardial trabeculation by secretion of growth factors such as
80 Neuregulin 1 (NRG1) and transforming growth factor ß (TGFß)[2, 3, 5]. Meanwhile, CECs
81 support trabeculation by secreting ECM (e.g., various collagens, versican) that facilitate
82 the travelling of CEC secreted growth factors to trabecular myocardium and support
83 trabecular CM proliferation[4, 7]. Surprisingly, disruption of ECM components alone (e.g.,
84 hyaluronan synthase-2, versican) prevents the proper formation of trabeculae in mice[8, 9].
85 Although CECs play such important roles during ventricular trabeculation, it remains
86 poorly understood how these ECM proteins and growth factors are regulated in the
87 developing CECs.

88 TGFß signaling pathway is involved in many fundamental cellular processes in both
89 adults and developing embryos including cell proliferation, differentiation, migration, and
90 apoptosis[10, 11]. The TGFß superfamily includes many different ligands (e.g., Bone
91 morphogenetic proteins, Growth and differentiation factors, Activin, Nodal, TGFß). These
92 ligands bind to their specific type II receptors, which triggers phosphorylation of type I
93 receptor, eventually leads to phosphor-Smad2/3 localized to the nucleus and drives a

94 variety of downstream target gene expression, which is the canonical TGFß signaling
95 pathway[12]. In addition, the binding of ligands to receptors can also directly activate
96 multiple non-Smad mediated intracellular signaling pathways such as MAP kinase
97 pathways and phosphatidylinositol-3-kinase/AKT pathways[13, 14]. These non-Smad
98 (noncanonical) TGFß signaling pathways are equally critical for driving some specific
99 cellular processes (e.g., cell proliferation, cell survival, endothelial/epithelial
100 mesenchymal transition)[13, 14]. During cardiovascular development, unsurprisingly, TGFß
101 signaling is implicated in most morphological events including cardiac lineage
102 specification, cardiac looping, valvogenesis, and cardiomyogenesis[15]. The TGFß family
103 includes TGFß1, TGFß2, and TGFß3. Although TGFß1, TGFß2 and TGFß3 are
104 abundantly expressed in the developing endocardium and epicardium, it appears that
105 they do not perform redundant functions: individual knockout results in different
106 phenotypes[15]. For instance, global knockout of either *Tgfß2* or *Tgfß3* result in early
107 perinatal lethality, presenting hypoplastic hearts with thin myocardium[15-17], suggesting
108 that they play critical roles for myocardial growth. In contrast, global knockout of *Tgfß1*
109 lead to partial embryonic lethality with survivors appearing phenotypically normal in first
110 the two weeks of life[18]. Nonetheless, it is poorly understood how the expression of TGFß
111 ligands are regulated in the early developing heart.
112 Epigenetic modulators such as histone deacetylases (HDACs) are critical for early heart
113 development as key regulators of regulating gene expresison[19]. There are 18 known
114 human HDACs, which can be subdivided into four classes based on their function and
115 DNA sequence similarity. Class I HDACs include HDAC1, HDAC2, HDAC3, and HDAC8,
116 and are predominantly nuclear and ubiquitously expressed[20, 21]. Although class I HDACs

117 have high degree of homology, global knockout of each causes early embryonic lethality[19],
118 suggesting distinct roles during early heart development. Global deletion of *Hdac3* leads
119 to early embryonic lethality at gastrulation[22]. In the developing heart, lack of *Hdac3* in
120 cardiac progenitors disrupts secondary heart field development[23], lymphovenous valve
121 morphogenesis[24], and CM lineage specification[25]. Recently, we reported that HDAC3 in
122 the developing epicardium plays a critical role in supporting compact myocardial wall
123 expansion[26]. It is unclear whether or how HDAC3 in the developing endocardium impacts
124 myocardial trabeculation.
125 In the current study, we investigated the role of HDAC3 in the developing endocardium
126 during early heart development.

127 **Materials and Methods**

128 ***Mice***

129 *Hdac3*$^{flox/+}$, *Tie2-Cre*, *Nfatc1*$^{Cre/+}$, *R26*^{eYFP} and *Tnnt2*$^{nGFP/+}$ mice were previously
130 described[27-31]. B6.Cg-Tg(*Tek-cre*)12Flv/J (abbreviated as *Tie2-Cre* in this manuscript),
131 *Hdac3*$^{flox/+}$, and *R26*^{eYFP} mice are available at the Jackson Laboratory (Stock numbers:
132 #004128, #024119 and #006148, respectively). All animal protocols were approved by
133 the Nationwide Children's Institutional Animal Care and Use Committee (IACUC).

134

135 ***Histology and immunofluorescence staining***

136 All embryo specimens were fixed in 4% paraformaldehyde overnight, dehydrated through
137 an ethanol series, paraffin embedded, and sectioned (6-7μm). Primary antibodies (Major
138 Resources Table) were incubated at 4°C overnight and secondary antibodies (Alexa 488
139 or Alexa 555, Thermo Fisher Scientific, Waltham, MA) were incubated at room
140 temperature for one hour. Stained slides were imaged on a Zeiss LSM 710 confocal
141 Microscope or a Leica DM6 fluorescence microscope. Epifluorescence and gross images
142 of embryos were imaged on a Leica M205 FCA stereo fluorescence microscope. The
143 number of phosphor-Histone 3 (p-H3)+ cells, Bromodeoxyuridine (BrdU)+ cells, and
144 TUNEL+ cells was quantified using ImageJ software.

145

146 ***Cell culture, transient transfection, lentiviral infection, and luciferase assay***

147 Mouse cardiac endothelial cells (MCECs) were purchased from Cedarlane Labs
148 (Catalogue #CLU510, Burlington, NC). MCECs were cultured in 10% fetal bovine serum
149 (FBS) supplemented DMEM at 37°C in a humidified incubator with 5% CO_2. To generate

150 stable *Hdac3* KO MCECs, as previously described[26], we cloned *Hdac3* sgRNA into
151 lentiCRISPR v2 vector (Addgene #52961; Watertown, MA). Seventy-percent confluent
152 Lenti-X™ 293T cells (Takara Bio USA, Inc., Mountain View, CA) were transfected with
153 *Hdac3* lentiviral plasmids (*Hdac3* KO or empty vector control [EV]), PsPAX2 (Addgene
154 #12260) and PMD2G (Addgene #12259). Seventy-two hours after transfection,
155 supernatants containing lentivirus were collected and filtered through a 40μm cell strainer.
156 MiR-129-5p mimics and scramble control mimics were custom-ordered from Dharmacon
157 (Lafayette, CO). MCECs were transfected with miR-129-5p mimics or control mimics (30
158 pmol) using Lipofectamine RNAiMAX (Thermo Fisher Scientific, Waltham, MA). 72 hours
159 after miR mimics treatment, supernatants were collected. miRZip anti-miR precursor
160 constructs for miRZip-129-5p and pGreenPuro Scramble Hairpin control constructs were
161 purchased from System Biosciences (Palo Alto, CA), and lentiviruses were generated
162 according to the manufacturer's protocol.
163
164 ***RNA isolation, quantitative real-time PCR (qRT-PCR), and bulk RNA-Seq***
165 MCECs and embryonic day (E) 11.5 hearts were used for RNA isolation. E11.5 hearts
166 were microdissected in cold PBS and snap frozen in liquid nitrogen. The RNeasy Plus
167 Mini Kit (QIAGEN, Germantown, MD) was used to extract total RNA, and cDNAs were
168 generated using the Superscript III kit (Thermo Fisher Scientific, Waltham, MA). To detect
169 mRNA, SYBR Green qRT-PCR was performed. PCR primers for genes of interest are
170 listed in Major Resources Table. To perform mature microRNA expression analyses,
171 purified total RNAs were converted to cDNAs using TaqMan™ MicroRNA Reverse
172 Transcription Kit (Catalogue #4366596, Thermo Fisher Scientific). qRT-PCR reactions

173 were run on StepOne Plus Real-Time PCR System (Applied Biosystems, Waltham, MA).
174 The probe sequences for mmu-miR-129-5p and U6 snRNA were purchased from Thermo
175 Fisher Scientific. For bulk RNA and miRNA-Sequencing, samples were prepared
176 following the provider's guidelines (Novogene Corporation Inc, Sacramento, CA) and
177 sequenced on an Illumina NextSeq500 (San Diego, CA). Sequencing reads were aligned
178 to the UCSC mm10 reference genome using tophat2 and bowtie2 in R. Differential
179 expression of transcripts was calculated using the cufflinks suite in R analyses.
180
181 ***Single cell RNA-Sequencing (scRNA-seq)***
182 E11.5 heart tissues were dissected in cold PBS and digested with 0.25% trypsin at 37°C
183 for 15 minutes. Digested cardiac cells were filtered with 70 μm cell strainers to remove
184 remaining clumps. Subsequently, 10,000 live cells were captured with Chromium Next
185 GEM Single Cell 3' Reagent Kits v3.1 (10X Genomics, Pleasanton, CA) following
186 manufacturer's instructions. Briefly, single cells were partitioned into nanoliter-scale Gel
187 Beads-in-emulsion (GEMs) using Chromium Next GEM Chip G in the chromium controller.
188 Immediately following GEM generation, the Gel Bead was dissolved, primers were
189 released, and co-partitioned cell was lysed, and its mRNA were reverse transcribed into
190 barcoded cDNA. After further cleanup and amplification, the cDNA was enzymatically
191 fragmented and amplified via PCR to generate sufficient mass for library construction.
192 After end repair, A-tailing, adaptor ligation and sample index PCR, the library comprised
193 constructs containing the sample index, UMI sequences, barcode sequences, and
194 Illumina standard sequencing primers P5 and P7 at both ends. The library was sequenced
195 with Illumina NextSeq S4 platform to a sequencing depth of 140-270 million reads per

196 sample. Reads were aligned to the Ensembl 104 mouse reference genome including the
197 sequence for eYFP as a separate contig using STARsolo (version 2.7.10b)[32]. The
198 resulting count tables (cells x genes) were converted into Annotated Data (anndata)
199 format for analysis in Python. For quality control, all cells with less than 1500 or more than
200 9000 genes expressed were excluded. Additionally, cell doublets were filtered out using
201 the Scrublet method[33]. Gene counts were normalized per cell to a total target sum and
202 transformed using log1p. Highly variable genes were identified using the Seurat method[34]
203 and these genes were utilized for dimension reduction with PCA. Finally, cell embedding
204 was performed with the UMAP algorithm (umap-learn version 0.5.3) and cells were
205 clustered using leiden (leidenalg version 0.9.1) with resolution 0.2. Scoring of trabecular
206 and compact CM subtypes was performed using 'score_genes' and differentially
207 expressed genes between groups were obtained using 'rank_genes_groups', both
208 methods from the SCANPY package[35].
209

210 ***Western blotting***

211 Cell or tissue lysates were prepared in lysis buffer (20 mM Tris-HCl [pH 7.5], 15 mM NaCl,
212 1 mM Na_2EDTA, 1 mM EGTA, 1% Triton X-100, 1 µg/ml leupeptin, 2.5 mM sodium
213 pyrophosphate, 1 mM Na_3VO_4, and 1 mM β-glycerophosphate) with protease inhibitor
214 cocktail (Roche, Indianapolis, IN) and 1 mM phenylmethylsulfonyl fluoride. Protein
215 samples were resolved on 4–12% SDS-PAGE acrylamide gels before transferring to
216 polyvinylidene fluoride membranes. Primary antibodies were visualized by
217 chemiluminescence using HRP-conjugated secondary antibodies. Antibodies are listed

218 in Major Resources Table. Western blots were normalized to loading controls and
219 densitometric analysis was performed using Image J software.
220
221 ***Statistical analysis***
222 All experiments were independently repeated at least three times, and the number of
223 samples (n) is stated in figure legends. Results are reported as the mean ± SD. For
224 statistical analyses, normal distribution of data was assessed by Shapiro-Wilk's test
225 (when n≥6). For data with small sample size (n<6), non-parametric tests were applied.
226 For parametric data with normal distribution, the statistical significance of the difference
227 between means was assessed using the unpaired two tailed Student's t-test between two
228 groups and the Tukey or Dunnett post hoc test for one-way ANOVA. For non-parametric
229 data or data with small sample size (n<6), the Mann-Whitney U test and Kruskal-Wallis
230 test for one-way ANOVA followed by the Dunn post hoc test were performed for
231 comparisons between two groups. Specific statistical tests are stated in figure legends.
232 RNA-seq data were background-corrected, variance-stabilized, normalized, and count
233 matrix extracted through quality control using lumi package for the R programming
234 language (http://bioconductor.org/packages/release/bioc/html/lumi.html). Differential
235 expression analysis was performed using DESeq2 R package
236 (https://bioconductor.org/packages/release/bioc/html/DESeq2. html). The resulting *p*-
237 values were adjusted using the Benjamini and Hochberg's approach for controlling the
238 False Discovery Rate (FDR)[36]. Genes or miRs with an adjusted *p*-value<0.05 found by
239 DESeq2 were assigned as differentially expressed. Gene ontology (GO) enrichment
240 analyses were performed using the Database for Annotation, Visualization and Integrated

241 Discovery (DAVID) bioinformatics resources (https://david.ncifcrf.gov/). For relative gene
242 expression analysis of qRT-PCR data, the expression of a gene of interest relative to an
243 internal loading control gene was calculated using the comparative CT method (-ΔΔCT)[37].
244 The relative protein expression on western blots was quantified by densitometry, Fold
245 changes for relative gene or protein expression were derived through division of values
246 in the experimental group by the mean values from the control group. *P*-value<0.05 was
247 considered statistically significant. All statistical analyses were performed using
248 GraphPad Prism 8 (GraphPad Prism software, Inc). The images with the value closest to
249 the mean value were selected as representative images.
250

251 **Results**

252 **Endothelial/Endocardial cell specific deletion of *Hdac3* results in embryonic**
253 **lethality and hypotrabeculation.**

254 To study the role of HDAC3 in the cardiac endothelium during early heart development,
255 *Hdac3* was specifically deleted in the endothelial cells using *Tie2-Cre*[28], while its
256 expression in other cells including CMs remains intact (Supplemental Figure 1). Note:
257 since *Tie2-Cre* is transiently expressed in oocytes[38], the mating scheme was always
258 *Hdac3*$^{f/+}$*; Tie2-Cre/+* (♂) and *Hdac3*$^{f/f}$ (♀). By recovering the progenies at a series of
259 embryonic and postnatal stages, we identified that *Hdac3* KO in the developing
260 endothelium resulted in early embryonic lethality starting at E12.5 (Supplemental Table
261 1). To investigate the potential cause of early embryonic lethality, we performed
262 histological analyses. Interestingly, in Tie2 endothelial *Hdac3* KO embryos (*Hdac3*^{tko}),
263 there was no noticeable phenotype in the various endothelial cell derived tissue where
264 the Tie2-lineage contributes, such as endocardium (Figure 1, Supplemental Figure 2) and
265 blood vessels (Supplemental Figure 3), given that *Tie2-Cre* is active in all endothelial cells
266 in the body[39]. In contrast, there were myocardial defects in *Hdac3*^{tko} embryos starting at
267 E11.5: *Hdac3*^{tko} trabeculae appeared to be significantly sparser and shorter as compared
268 to the thick and long webbing like trabecular network in littermate control hearts
269 (Supplemental Figure 2). This cardiac phenotype in *Hdac3*^{tko} mice was more prominent
270 at E12.5 (Figure 1A). The compact layer was thinner (not significant) in *Hdac3*^{tko} hearts.
271 To further validate the myocardial trabecular phenotype in endothelial *Hdac3* deleted
272 hearts, we specifically deleted *Hdac3* in the endocardium using *Nfatc1*$^{Cre/+}$, endocardial
273 specific Cre[29], which also resulted in embryonic lethality (Supplemental Table 2).

274 *Hdac3*^{nko} (*Hdac3*$^{f/f}$*; Nfatc1*$^{Cre/+}$) hearts presented a similar cardiac phenotype, albeit at a
275 later stage (E14.5): smaller and sparser trabeculae, thinner compact wall (Supplemental
276 Figure 4). This is consistent with the achievement of late deletion of *Hdac3* in the
277 endocardium by *Nfatc1*$^{Cre/+}$ (Supplemental Figure 4). Nonetheless, these results confirm
278 that the cardiac phenotypes resulting from *Tie2* endothelial *Hdac3* deletion are primarily
279 from the endocardium, and not secondary to another endothelium (e.g., vascular).
280 *Hdac3*^{tko} embryos were used for all subsequent mechanistic studies.
281
282 **Endothelial *Hdac3* knockout hearts display decreased trabecular CM proliferation.**
283 Next, we investigated whether altered cell proliferation and/or apoptosis contribute to the
284 hypotrabeculation phenotypes in *Hdac3*^{tko} hearts. At E11.5, the percentage of p-H3+ CMs
285 is significantly lower in *Hdac3*^{tko} myocardium as compared to littermate control hearts
286 (Figure 1B). This finding is consistent with the hypoplastic cardiac phenotypes seen in
287 *Hdac3*^{tko} hearts (Figure 1A). In contrast, there was no significant difference in cell
288 apoptosis between *Hdac3*^{tko} hearts and littermate control hearts (Supplemental Figure 5).
289 Decreased CM proliferation of *Hdac3*^{tko} hearts may result from disrupted communication
290 from the endocardium to the trabecular myocardium. We performed single cell RNA-
291 sequencing (scRNA-seq) on E11.5 *Hdac3*^{tko} hearts and littermate control hearts (Figure
292 2A). We obtained high-quality scRNA-seq profiles for 23,468 and 25,547 cells from 4
293 *Hdac3*^{tko} (*Hdac3*$^{f/f}$*; Tie2-Cre/+; R26*$^{eYFP/+}$) and 4 control (3 of *Hdac3*$^{f/+}$*; Tie2-Cre/+;*
294 *R26*$^{eYFP/+}$ and 1 of *Hdac3*$^{f/+}$*; Tie2-Cre/+*) heart single cell suspensions, respectively.
295 Unsupervised clustering successfully separated 6 distinct clusters including endocardial
296 cells and CMs in these samples (Figure 2B). Referring to a recent transcriptome profiling

297 methodology for clustering embryonic CMs[40], we re-clustered CMs into “trabecular” and
298 “compact” clusters based on the overall scores after applying a few known trabecular and
299 compact markers (trabecular: *Bmp10*, *Nppa* and *Thbs4*; compact: *Hey2*, *Mycn* and *Tnnt1*)
300 (Supplemental Figure 7 and Figure 2C). Among them, *Bmp10*+ CMs nicely represent the
301 trabecular cluster (Figure 2C), and thus we focused on this population for subsequent
302 analyses since *Hdac3*^{tko} hearts display hypotrabeculation phenotypes (Figure 1). Overall,
303 the total number of trabecular CMs were not significantly different between *Hdac3*^{tko} and
304 littermate control hearts (Supplemental Figure 6A). Note: 10,000 cells/sample was
305 sequenced. Next, we performed differential gene expression (DGE) analyses on *Hdac3*^{tko}
306 and littermate control trabecular clusters. We found that the expression of eukaryotic
307 translation elongation factor 1 alpha 2 (*Eef1a2*) and early growth response-1 (*Egr-1*) are
308 significantly down regulated in *Hdac3*^{tko} trabeculae as compared to control trabeculae
309 (Figure 2D). *Eef1a2* and *Egr1* are known to be critical for cell growth[41-43]. These findings
310 are consistent with reduced proliferation index seen in *Hdac3*^{tko} hearts (Figure 1B),
311 suggesting myocardial growth retardation account for the hypotrabeculation phenotypes
312 in *Hdac3*^{tko} hearts.
313
314 **Endothelial HDAC3 induces ECM gene expression.**
315 Among all scRNA-seq samples, 7 of them carried *R26*$^{eYFP/+}$ reporters (3 CTL and 4
316 *Hdac3*^{tko}). This enabled us to perform a lineage specific analysis. In the single cell
317 suspension, 8.6% cells in CTL hearts and 11.2% cells in *Hdac3*^{tko} hearts were YFP+
318 (Supplemental Figure 6B). During early heart development, endothelial progenitors can
319 also give rise to fibroblasts/mesenchymal cells through endothelial to mesenchymal

320 transition[6, 44]. As expected, YFP+ cells (Tie2 lineage) were primarily CECs with a minority
321 of fibroblasts (Figure 2E). Also, as expected, *Hdac3* expression was absent in *Hdac3*^{tko}
322 YFP+ cells. Subsequent DGE analysis did not reveal significant gene expression
323 differences between *Hdac3*^{tko} and control fibroblasts (Figure 2E). Instead, in CEC clusters,
324 we found that the expression of genes regulating cellular component organization was
325 highly enriched in the control YFP+ CEC cluster (Figure 2F). In particular, the expression
326 of ECM associated genes, including *Col13a1, Col1a2, Tgfbi, Timp2, Col26a1, Col3a1,*
327 *Col4a5*, *Timp3*, and *P4ha3*, was significantly reduced in *Hdac3*^{tko} YFP+ CEC cluster as
328 compared to control YFP+ CEC cluster (Figure 2G). *Col1a1, Col1a2, Col2a1*, and *Col3a1*
329 and *P4ha3* DGE was further validated in *Hdac3*^{tko} and control heart lysates by qRT-PCR
330 (Figure 2H). These results suggest that cardiac endothelial HDAC3 induces the
331 expression of ECM associated genes, which are critical for CM proliferation and
332 trabeculation growth (Figure 2I).
333
334 **Cardiac endothelial HDAC3 induces *Tgfβ3* in driving CM proliferation.**
335 Trabeculation and ECM remodeling are coordinated during early heart development, and
336 both processes are regulated by growth signaling[45]. To better identify potential growth
337 signaling pathways regulated by HDAC3 in the endocardium, we used a mouse cardiac
338 endothelial cell (MCEC) line[46]. Using CRISPR-Cas9 gene editing technology and the
339 same set of gRNAs we have recently used[26], we successfully knocked out *Hdac3* in the
340 MCECs (Figure 3A). *Hdac3* KO MCECs grew slower than *Hdac3* empty vector (EV)
341 control MCECs. To determine whether the secretome from *Hdac3* KO endothelial cells is
342 competent to induce CM proliferation, we treated cultured primary embryonic CMs

343 isolated from E13.5 *Tnnt2*$^{nGFP/+31}$ hearts with supernatant from either *Hdac3* KO MCECs
344 or *Hdac3* EV MCECs, respectively. *Hdac3* KO supernatant treatment resulted in
345 significant decrease of the percentage of p-H3+ CMs and the total number of CMs, as
346 compared to *Hdac3* EV supernatant treatment (Figure 3B). These results suggest that
347 growth signals derived from CECs required to support CM proliferation may be
348 inadequate/deficient in *Hdac3* KO MCECs. To unbiasedly search for such growth signals,
349 we performed bulk RNA-Seq analyses on *Hdac3* KO and EV MCECs; we identified 484
350 downregulated and 239 upregulated genes. Gene ontology pathway analyses revealed
351 that a number of endocardium-initiated signaling pathways were significantly
352 downregulated in *Hdac3* KO MCECs (Supplemental Figure 8A). Through DGE analysis,
353 we found that growth factors including *Igf1, Tgfβ3, Tgfβ2, Tgfβ1, Igf1, Cxcl12, Nrg1 and*
354 *Vegfβ* were significantly downregulated in *Hdac3* KO MCECs (Supplemental Figure 8B).
355 We attempted to validate these results at the protein level by western blot. Surprisingly,
356 we found that only TGFβ3 protein expression was significantly decreased in *Hdac3* KO
357 MCECs as compared to *Hdac3* EV MCECs (Supplemental Figure 8C), and thus we chose
358 TGFβ3 to pursue further. Interestingly, TGFβ3 was also significantly decreased when the
359 deacetylase activity of HDAC3 was inhibited by RGFP966 (a HDAC3 selective inhibitor)
360 treatment (Figure 3C and Supplemental Figure 9D). TGFβ3 was also significantly
361 downregulated in E11.5 *Hdac3*^{tko} hearts compared to littermate CTL hearts (Figure 3D).
362 Next, we determined whether TGFβ3 deficiency in *Hdac3* KO MCECs contributed to the
363 CM proliferation deficit following *Hdac3* KO supernatant treatment. First, we quantified
364 TGFβ3 and showed that it was significantly decreased in the supernatants from *Hdac3*
365 KO MCECs compared to that from *Hdac3* EV MCECs (Figure 3E). Next, we evaluated

366 CM proliferation after we supplemented *Hdac3* KO supernatants with recombinant mouse
367 TGFβ3 protein. Strikingly, TGFβ3 supplementation successfully rescued CM proliferation
368 defects by *Hdac3* KO supernatant treatment (Figure 3F). These results suggest that
369 cardiac endothelial HDAC3 supports CM proliferation by inducing *Tgfβ3* expression.
370

371 **Cardiac endothelial HDAC3 induces *Tgfβ3* expression through repressing**
372 **microRNA (miR)-129-5p.**

373 Recently, we reported that HDAC3 regulates growth factors by modulating the miR
374 pathway in the developing epicardium[26]. To identify the potential HDAC3 downstream
375 miR targets in CECs, we performed miR sequencing in *Hdac3* KO and EV MCECs.
376 Through DGE analyses, we found that 5 miRs were significantly upregulated in *Hdac3*
377 KO MCECs (Figure 4A) (cutoff threshold: Log2 fold change greater than 1.5 and adjusted
378 $P<0.01$). To identify which miR(s) may regulate *Tgfβ3* expression, we treated MCECs
379 with mimics of each of the 5 miRs and found that treatment with miR-129-5p mimics
380 significantly inhibited the expression of *Tgfβ3* (Figure 4B). This finding was validated by
381 western blot (Figure 4C). We further validated the upregulation of miR-129-5p in both
382 *Hdac3* KO MCECs and E11.5 *Hdac3*^{tko} hearts (Figure 4D and 4E). Interestingly, miR-
383 129-5p was similarly significantly upregulated when the deacetylase activity of HDAC3 is
384 inhibited by RGFP966 treatment (Figure 4F), suggesting the inhibition of miR-129-5p
385 expression by HDAC3 is deacetylase dependent. Lastly, to determine whether HDAC3
386 induces *Tgfβ3* expression through repressing miR-129-5p, we knocked down miR-129-
387 5p by miRZip lentivirus in *Hdac3* KO MCECs. Remarkably, miR-129-5p knockdown
388 significantly restored the *Tgfβ3* expression in *Hdac3* KO MCECs (Figure 4G). These

389 results suggest that HDAC3 promotes the expression of TGFβ3 through repressing miR-

390 129 in supporting trabecular CM proliferation (Figure 4H).

391 **Discussion**

392 Myocardial growth/expansion, one of the most critical cardiac developmental events, is
393 accompanied by two separate but closely associated processes: compaction and
394 trabeculation. Many forms of congenital heart disease are associated with abnormal
395 cardiac trabeculation and compaction[2, 3]. For proper myocardial development, besides
396 cardiomyocytes, the surrounding non-cardiomyocytes including endocardial cells can
397 influence myocardial growth by sending growth signals to the neighboring myocardia[47],
398 as well as secreting ECM proteins that serve as signal transmission media[2, 48]

399 Epigenetic regulation can define a tissue-specific and developmental stage-specific
400 transcription network during early heart development[49, 50], mainly achieved by
401 posttranslational modifications of histones, around which DNA winds. There are several
402 different types of histone modifications (e.g., methylation/demethylation,
403 acetylation/deacetylation, phosphorylation/dephosphorylation, ubiquitination/
404 deubiquitination). By alternating between any of these states, the associated genes can
405 be dynamically poised to be transcriptionally active/repressed. Histone deacetylases
406 (HDACs) are family of enzymes that remove acetyl groups from a lysine residue on a
407 histone, allowing the histones to wrap the DNA more tightly to repress gene expression.
408 Class I HDACs, includes HDAC3, are widely expressed, but play specific roles during
409 early embryogenesis and organogenesis[19]. Mesodermal or global knockout of *Hdac3*
410 results in myogenic defects and early embryonic lethality[22, 51]. Interestingly, specific
411 deletion of *Hdac3* in the myocardium does not generate cardiac morphogenic phenotypes
412 during early heart development, but rather compromises cardiac function at later
413 postnatal stages[51, 52]. These early findings suggest that the function of HDAC3 in

414 nonmyocyte compartments may be critical for early cardiac morphogenesis and
415 myocardial development. Our recent work demonstrated that epicardial HDAC3 is critical
416 for driving myocardial compact wall expansion[26]. Our current study suggests that
417 endocardial HDAC3 is important for myocardial trabeculation: endothelial/endocardial
418 deletion of *Hdac3* resulted in hypotrabeculation (Figure 1 and Supplemental Figure 4).
419 We note that *Tie2-Cre* turns on around E8.0-8.5 in all endothelial cells[39], whereas
420 *Nfatc1*$^{Cre/+}$ is active around E9.5 only in endocardial cells[29] and only achieves efficient
421 *Hdac3* deletion by E14.5 likely due to inefficient IRES-mediated Cre transcription[53]
422 (Supplemental Figure 4). Nonetheless, these two deletion models generated similar
423 cardiac phenotypes of hypotrabeculation, although we did observe differences in the
424 severity of the myocardial phenotypes and time of lethality, which we attribute to the
425 different temporal and spatial activities and/or efficiencies of these two Cres. An earlier
426 report of conditional deletion of *Hdac3* in endothelial cells using a different Tie2-Cre driver
427 primarily targeting hemogenic endothelial cells[28] resulted in mid-gestational lethality
428 (E14.5) presenting predominantly a lymphovenous and lymphatic valve malformation
429 phenotype[54]. However, it is unknown what phenotypes were present in the myocardium
430 in that study as none were reported. Nonetheless, we deemed it inapplicable to evaluate
431 potential lymphatic valve phenotypes in our pan-endothelial *Hdac3* KO embryos since
432 these mice died around E12.5 (Supplemental Table 1), while lymphovenous and
433 lymphatic valve formation starts at E13.5[55]. However, it is interesting to note that the role
434 of HDAC1 and HDAC2 in the developing endocardium appears to be dispensable, as
435 deletion of either *Hdac1* or *Hdac2* by Tie2-Cre do not elicit apparent cardiac phenotypes[24].

436 These results suggest that HDAC3 plays distinctive roles from HDAC1 and HDAC2,
437 although they share high homology and are grouped in the same HDAC subfamily[19].
438 TGFß signaling is involved in many processes during early heart development such as
439 ECM production, endothelial to mesenchymal transition, and myogenesis[11, 56-58].
440 Specifically, TGFß signaling plays an instrumental role in trabeculation[59-62]. For instance,
441 knockout of either TGFß2 or TGFß3 results in hypoplastic ventricular myocardium[15]. We
442 found that TGFß3 expression was significantly decreased in *Hdac3* deleted endocardium
443 (Figure 3). Interestingly, inhibition of deacetylase activity of HDAC3 alone significantly
444 decreased TGFß3 expression. Further, supplementation of TGFß3 to cardiac endothelial
445 Hdac3 KO secretome significantly rescued cardiomyocyte proliferation defect (Figure 3F),
446 suggesting that cardiac endothelial HDAC3 supports trabeculation through inducing
447 TGFß3 in a deacetylase dependent manner. Interestingly, HDAC3 is also reported to
448 inhibit TGFß1 expression in the second heart field development in a deacetylase
449 independent manner[23], whereas HDAC3 deteriorates colorectal cancer progression by
450 inducing TGFß1 through inhibiting miR-296[63]. These divergent findings illustrate that
451 HDAC3 can either promote or inhibit TGFß signaling pathway through different molecular
452 mechanisms in a tissue/cell dependent manner.
453 Besides functioning as growth signals to cardiomyocytes, TGFß signaling is
454 predominantly known for its induction on ECMs[57, 64]. During early heart development,
455 ECM is mainly secreted from endocardium and mediates signal transduction from
456 endocardium to myocardium supporting trabeculation[63]. Our scRNA-Seq data revealed
457 that ECM is significantly down regulated in *Hdac3* endothelial KO hearts (Figure 2).
458 P4ha3, a major enzyme for collagen synthesis[65, 66] and a TGFß downstream target[67], was

459 also significantly decreased in *Hdac3* endothelial knockout hearts (Figure 2). These
460 results suggest that ECM downregulation may be secondary to decreased TGFß
461 signaling to contribute to the hypotrabeculation phenotypes in *Hdac3*
462 endothelial/endocardial knockout hearts.

463 We identified that HDAC3 suppresses miR-129-5p in inducing TGFß3 (Figure 4). miR-
464 129-5p plays important roles in cancer by either promoting or inhibiting tumorigenesis
465 through regulating a variety of downstream targets and pathways[68, 69]. Several studies
466 have shown that miR-129-5p protects adult hearts from ischemia/reperfusion injuries[70,
467 71], while another study demonstrated that treating cultured H9c2 cardiomyocytes with
468 HDAC pan-inhibitor Trichostatin A results in decreased cardiomyocyte proliferation with
469 enhanced miR-129-5p epression[72]. This is consistent with our current findings in the
470 developing endocardium (Figure 4). In our recent study, we found that HDAC3 induces
471 the expression of IGF2 and FGF9 by suppressing miR-322/503 in the developing
472 epicardium[26]. Again, these findings altogether suggest that HDAC3 can induce different
473 sets of growth signals by switching their downstream miR targets in a tissue/cell context
474 dependent manner.

475 In summary, our current study demonstrates that endocardial HDAC3 promotes
476 myocardial trabeculation by inducing TGFß signaling through repressing miR-129-5p
477 during early heart development. This finding, along with others, exemplifies the
478 importance of endocardial signaling for driving myocardial morphogenesis, and thus
479 provides new insights on the pathogenesis of congenital heart disease. The dual
480 epigenetic inhibition mechanism may be leveraged in some other contexts such as adult
481 heart repair/regeneration.

482 **Acknowledgments**

483 We thank Dr. Dennis Lewandowski in the Heart Center at the Nationwide Children's
484 Hospital for his critical reading and editing of the manuscript.

485

486 **Sources of Funding**

487 This work was partially supported by the National Heart, Lung, and Blood Institute R01
488 grant HL153406 (D. Li) and American Heart Association-Career Development Award
489 23CDA1046244 (J. Jang).

490

491 **Disclosure**

492 None.

493

494 **References:**

495 1. Zaidi S and Brueckner M. Genetics and Genomics of Congenital Heart Disease.
496 *Circulation research*. 2017;120:923-940.

497 2. Qu X, Harmelink C and Baldwin HS. Endocardial-Myocardial Interactions During Early
498 Cardiac Differentiation and Trabeculation. *Front Cardiovasc Med*. 2022;9:857581.

499 3. Wu M. Mechanisms of Trabecular Formation and Specification During Cardiogenesis.
500 *Pediatric cardiology*. 2018;39:1082-1089.

501 4. Lin W and Li D. Zinc and Zinc Transporters: Novel Regulators of Ventricular Myocardial
502 Development. *Pediatric cardiology*. 2018;39:1042-1051.

503 5. Zhang W, Chen H, Qu X, Chang CP and Shou W. Molecular mechanism of ventricular
504 trabeculation/compaction and the pathogenesis of the left ventricular noncompaction
505 cardiomyopathy (LVNC). *American journal of medical genetics Part C, Seminars in medical*
506 *genetics*. 2013;163C:144-56.

507 6. Zhang H, Lui KO and Zhou B. Endocardial Cell Plasticity in Cardiac Development,
508 Diseases and Regeneration. *Circulation research*. 2018;122:774-789.

509 7. Andries LJ, Sys SU and Brutsaert DL. Morphoregulatory interactions of endocardial
510 endothelium and extracellular material in the heart. *Herz*. 1995;20:135-45.

511 8. Camenisch TD, Spicer AP, Brehm-Gibson T, Biesterfeldt J, Augustine ML, Calabro A, Jr.,
512 Kubalak S, Klewer SE and McDonald JA. Disruption of hyaluronan synthase-2 abrogates normal
513 cardiac morphogenesis and hyaluronan-mediated transformation of epithelium to mesenchyme.
514 *J Clin Invest*. 2000;106:349-60.

515 9. Hatano S, Kimata K, Hiraiwa N, Kusakabe M, Isogai Z, Adachi E, Shinomura T and
516 Watanabe H. Versican/PG-M is essential for ventricular septal formation subsequent to cardiac
517 atrioventricular cushion development. *Glycobiology*. 2012;22:1268-77.

518 10. Chen JL, Colgan TD, Walton KL, Gregorevic P and Harrison CA. The TGF-beta Signalling
519 Network in Muscle Development, Adaptation and Disease. *Adv Exp Med Biol*. 2016;900:97-131.

520 11. Sorensen DW and van Berlo JH. The Role of TGF-beta Signaling in Cardiomyocyte
521 Proliferation. *Curr Heart Fail Rep*. 2020;17:225-233.
522 12. Zhang Y and Yang X. The Roles of TGF-beta Signaling in Cerebrovascular Diseases.
523 *Front Cell Dev Biol*. 2020;8:567682.
524 13. Moustakas A and Heldin CH. Non-Smad TGF-beta signals. *J Cell Sci*. 2005;118:3573-84.
525 14. Zhang YE. Non-Smad pathways in TGF-beta signaling. *Cell Res*. 2009;19:128-39.
526 15. Azhar M, Schultz Jel J, Grupp I, Dorn GW, 2nd, Meneton P, Molin DG, Gittenberger-de
527 Groot AC and Doetschman T. Transforming growth factor beta in cardiovascular development
528 and function. *Cytokine Growth Factor Rev*. 2003;14:391-407.
529 16. Koo SH, Cunningham MC, Arabshahi B, Gruss JS and Grant JH, 3rd. The transforming
530 growth factor-beta 3 knock-out mouse: an animal model for cleft palate. *Plast Reconstr Surg*.
531 2001;108:938-48; discussion 949-51.
532 17. Sanford LP, Ormsby I, Gittenberger-de Groot AC, Sariola H, Friedman R, Boivin GP,
533 Cardell EL and Doetschman T. TGFbeta2 knockout mice have multiple developmental defects
534 that are non-overlapping with other TGFbeta knockout phenotypes. *Development*.
535 1997;124:2659-70.
536 18. Kulkarni AB and Karlsson S. Transforming growth factor-beta 1 knockout mice. A mutation
537 in one cytokine gene causes a dramatic inflammatory disease. *Am J Pathol*. 1993;143:3-9.
538 19. Haberland M, Montgomery RL and Olson EN. The many roles of histone deacetylases in
539 development and physiology: implications for disease and therapy. *Nature reviews Genetics*.
540 2009;10:32-42.
541 20. Wright LH and Menick DR. A class of their own: exploring the nondeacetylase roles of
542 class IIa HDACs in cardiovascular disease. *Am J Physiol Heart Circ Physiol*. 2016;311:H199-206.
543 21. Wang Z, Zhao YT and Zhao TC. Histone deacetylases in modulating cardiac disease and
544 their clinical translational and therapeutic implications. *Exp Biol Med (Maywood)*. 2021;246:213-
545 225.

546 22. Bhaskara S, Chyla BJ, Amann JM, Knutson SK, Cortez D, Sun ZW and Hiebert SW.
547 Deletion of histone deacetylase 3 reveals critical roles in S phase progression and DNA damage
548 control. *Mol Cell*. 2008;30:61-72.
549 23. Lewandowski SL, Janardhan HP and Trivedi CM. Histone Deacetylase 3 Coordinates
550 Deacetylase-independent Epigenetic Silencing of Transforming Growth Factor-beta1 (TGF-
551 beta1) to Orchestrate Second Heart Field Development. *The Journal of biological chemistry*.
552 2015;290:27067-27089.
553 24. Janardhan HP, Milstone ZJ, Shin M, Lawson ND, Keaney JF, Jr. and Trivedi CM. Hdac3
554 regulates lymphovenous and lymphatic valve formation. *J Clin Invest*. 2017;127:4193-4206.
555 25. Poleshko A, Shah PP, Gupta M, Babu A, Morley MP, Manderfield LJ, Ifkovits JL, Calderon
556 D, Aghajanian H, Sierra-Pagan JE, Sun Z, Wang Q, Li L, Dubois NC, Morrisey EE, Lazar MA,
557 Smith CL, Epstein JA and Jain R. Genome-Nuclear Lamina Interactions Regulate Cardiac Stem
558 Cell Lineage Restriction. *Cell*. 2017;171:573-587 e14.
559 26. Jang J, Song G, Pettit SM, Li Q, Song X, Cai CL, Kaushal S and Li D. Epicardial HDAC3
560 Promotes Myocardial Growth Through a Novel MicroRNA Pathway. *Circulation research*.
561 2022;131:151-164.
562 27. Mullican SE, Gaddis CA, Alenghat T, Nair MG, Giacomin PR, Everett LJ, Feng D, Steger
563 DJ, Schug J, Artis D and Lazar MA. Histone deacetylase 3 is an epigenomic brake in macrophage
564 alternative activation. *Genes & development*. 2011;25:2480-8.
565 28. Koni PA, Joshi SK, Temann UA, Olson D, Burkly L and Flavell RA. Conditional vascular
566 cell adhesion molecule 1 deletion in mice: impaired lymphocyte migration to bone marrow. *The*
567 *Journal of experimental medicine*. 2001;193:741-54.
568 29. Wu B, Zhang Z, Lui W, Chen X, Wang Y, Chamberlain AA, Moreno-Rodriguez RA,
569 Markwald RR, O'Rourke BP, Sharp DJ, Zheng D, Lenz J, Baldwin HS, Chang CP and Zhou B.
570 Endocardial cells form the coronary arteries by angiogenesis through myocardial-endocardial
571 VEGF signaling. *Cell*. 2012;151:1083-96.

572 30. Srinivas S, Watanabe T, Lin CS, William CM, Tanabe Y, Jessell TM and Costantini F. Cre
573 reporter strains produced by targeted insertion of EYFP and ECFP into the ROSA26 locus. *BMC*
574 *Dev Biol*. 2001;1:4.
575 31. Yan J, Zhang L, Sultana N, Oh JG, Wu B, Hajjar RJ, Zhou B and Cai CL. A series of robust
576 genetic indicators for definitive identification of cardiomyocytes. *J Mol Cell Cardiol*. 2016;97:278-
577 85.
578 32. Dobin A, Davis CA, Schlesinger F, Drenkow J, Zaleski C, Jha S, Batut P, Chaisson M and
579 Gingeras TR. STAR: ultrafast universal RNA-seq aligner. *Bioinformatics*. 2013;29:15-21.
580 33. Wolock SL, Lopez R and Klein AM. Scrublet: Computational Identification of Cell Doublets
581 in Single-Cell Transcriptomic Data. *Cell Syst*. 2019;8:281-291 e9.
582 34. Satija R, Farrell JA, Gennert D, Schier AF and Regev A. Spatial reconstruction of single-
583 cell gene expression data. *Nat Biotechnol*. 2015;33:495-502.
584 35. Wolf FA, Angerer P and Theis FJ. SCANPY: large-scale single-cell gene expression data
585 analysis. *Genome Biol*. 2018;19:15.
586 36. Wang L, Feng Z, Wang X, Wang X and Zhang X. DEGseq: an R package for identifying
587 differentially expressed genes from RNA-seq data. *Bioinformatics*. 2010;26:136-8.
588 37. Schmittgen TD and Livak KJ. Analyzing real-time PCR data by the comparative C(T)
589 method. *Nature protocols*. 2008;3:1101-8.
590 38. de Lange WJ, Halabi CM, Beyer AM and Sigmund CD. Germ line activation of the Tie2
591 and SMMHC promoters causes noncell-specific deletion of floxed alleles. *Physiol Genomics*.
592 2008;35:1-4.
593 39. Kisanuki YY, Hammer RE, Miyazaki J, Williams SC, Richardson JA and Yanagisawa M.
594 Tie2-Cre transgenic mice: a new model for endothelial cell-lineage analysis in vivo. *Dev Biol*.
595 2001;230:230-42.

596 40. Wu T, Liang Z, Zhang Z, Liu C, Zhang L, Gu Y, Peterson KL, Evans SM, Fu XD and Chen
597 J. PRDM16 Is a Compact Myocardium-Enriched Transcription Factor Required to Maintain
598 Compact Myocardial Cardiomyocyte Identity in Left Ventricle. *Circulation*. 2022;145:586-602.
599 41. Hassan MK, Kumar D, Patel SA and Dixit M. EEF1A2 triggers stronger ERK mediated
600 metastatic program in ER negative breast cancer cells than in ER positive cells. *Life Sci*.
601 2020;262:118553.
602 42. Fish JE, Cantu Gutierrez M, Dang LT, Khyzha N, Chen Z, Veitch S, Cheng HS, Khor M,
603 Antounians L, Njock MS, Boudreau E, Herman AM, Rhyner AM, Ruiz OE, Eisenhoffer GT,
604 Medina-Rivera A, Wilson MD and Wythe JD. Dynamic regulation of VEGF-inducible genes by an
605 ERK/ERG/p300 transcriptional network. *Development*. 2017;144:2428-2444.
606 43. Thornton S, Anand N, Purcell D and Lee J. Not just for housekeeping: protein initiation
607 and elongation factors in cell growth and tumorigenesis. *J Mol Med (Berl)*. 2003;81:536-48.
608 44. Anbara T, Sharifi M and Aboutaleb N. Endothelial to Mesenchymal Transition in the
609 Cardiogenesis and Cardiovascular Diseases. *Curr Cardiol Rev*. 2020;16:306-314.
610 45. Del Monte-Nieto G, Ramialison M, Adam AAS, Wu B, Aharonov A, D'Uva G, Bourke LM,
611 Pitulescu ME, Chen H, de la Pompa JL, Shou W, Adams RH, Harten SK, Tzahor E, Zhou B and
612 Harvey RP. Control of cardiac jelly dynamics by NOTCH1 and NRG1 defines the building plan for
613 trabeculation. *Nature*. 2018;557:439-445.
614 46. Barbieri SS and Weksler BB. Tobacco smoke cooperates with interleukin-1beta to alter
615 beta-catenin trafficking in vascular endothelium resulting in increased permeability and induction
616 of cyclooxygenase-2 expression in vitro and in vivo. *FASEB J*. 2007;21:1831-43.
617 47. Tian Y and Morrisey EE. Importance of myocyte-nonmyocyte interactions in cardiac
618 development and disease. *Circulation research*. 2012;110:1023-34.
619 48. Silva AC, Pereira C, Fonseca A, Pinto-do OP and Nascimento DS. Bearing My Heart: The
620 Role of Extracellular Matrix on Cardiac Development, Homeostasis, and Injury Response. *Front*
621 *Cell Dev Biol*. 2020;8:621644.

622 49. Paige SL, Thomas S, Stoick-Cooper CL, Wang H, Maves L, Sandstrom R, Pabon L,
623 Reinecke H, Pratt G, Keller G, Moon RT, Stamatoyannopoulos J and Murry CE. A temporal
624 chromatin signature in human embryonic stem cells identifies regulators of cardiac development.
625 *Cell*. 2012;151:221-32.
626 50. Wamstad JA, Alexander JM, Truty RM, Shrikumar A, Li F, Eilertson KE, Ding H, Wylie JN,
627 Pico AR, Capra JA, Erwin G, Kattman SJ, Keller GM, Srivastava D, Levine SS, Pollard KS,
628 Holloway AK, Boyer LA and Bruneau BG. Dynamic and coordinated epigenetic regulation of
629 developmental transitions in the cardiac lineage. *Cell*. 2012;151:206-20.
630 51. Lewandowski SL, Janardhan HP and Trivedi CM. Histone Deacetylase 3 Coordinates
631 Deacetylase-independent Epigenetic Silencing of Transforming Growth Factor-beta1 (TGF-
632 beta1) to Orchestrate Second Heart Field Development. *The Journal of biological chemistry*.
633 2015;290:27067-89.
634 52. Montgomery RL, Potthoff MJ, Haberland M, Qi X, Matsuzaki S, Humphries KM,
635 Richardson JA, Bassel-Duby R and Olson EN. Maintenance of cardiac energy metabolism by
636 histone deacetylase 3 in mice. *J Clin Invest*. 2008;118:3588-97.
637 53. Artap S, Manderfield LJ, Smith CL, Poleshko A, Aghajanian H, See K, Li L, Jain R and
638 Epstein JA. Endocardial Hippo signaling regulates myocardial growth and cardiogenesis. *Dev*
639 *Biol*. 2018;440:22-30.
640 54. Celikyurt U, Karauzum K, Sahin T, Agacdiken A, Vural A and Ural D. Association between
641 resolution of fragmented QRS and response to cardiac resynchronization therapy. *Ann*
642 *Noninvasive Electrocardiol*. 2015;20:126-31.
643 55. Yang Y and Oliver G. Development of the mammalian lymphatic vasculature. *J Clin Invest*.
644 2014;124:888-97.
645 56. Conway SJ, Doetschman T and Azhar M. The inter-relationship of periostin, TGF beta,
646 and BMP in heart valve development and valvular heart diseases. *ScientificWorldJournal*.
647 2011;11:1509-24.

648 57. Frangogiannis NG. Transforming growth factor-beta in myocardial disease. *Nat Rev*
649 *Cardiol*. 2022;19:435-455.
650 58. Lee JH and Massague J. TGF-beta in developmental and fibrogenic EMTs. *Semin Cancer*
651 *Biol*. 2022;86:136-145.
652 59. Chakrabarti M, Al-Sammarraie N, Gebere MG, Bhattacharya A, Chopra S, Johnson J,
653 Pena EA, Eberth JF, Poelmann RE, Gittenberger-de Groot AC and Azhar M. Transforming
654 Growth Factor Beta3 is Required for Cardiovascular Development. *J Cardiovasc Dev Dis*. 2020;7.
655 60. Dunker N and Krieglstein K. Tgfbeta2 -/- Tgfbeta3 -/- double knockout mice display severe
656 midline fusion defects and early embryonic lethality. *Anat Embryol (Berl)*. 2002;206:73-83.
657 61. Kruithof BP, Kruithof-De-Julio M, Poelmann RE, Gittenberger-De-Groot AC, Gaussin V
658 and Goumans MJ. Remodeling of the myocardium in early trabeculation and cardiac valve
659 formation; a role for TGFbeta2. *Int J Dev Biol*. 2013;57:853-63.
660 62. Kodo K, Ong SG, Jahanbani F, Termglinchan V, Hirono K, InanlooRahatloo K, Ebert AD,
661 Shukla P, Abilez OJ, Churko JM, Karakikes I, Jung G, Ichida F, Wu SM, Snyder MP, Bernstein D
662 and Wu JC. iPSC-derived cardiomyocytes reveal abnormal TGF-beta signalling in left ventricular
663 non-compaction cardiomyopathy. *Nat Cell Biol*. 2016;18:1031-42.
664 63. Li J, Hu M, Liu N, Li H, Yu Z, Yan Q, Zhou M, Wang Y, Song Y, Pan G, Liang F and Chen
665 R. HDAC3 deteriorates colorectal cancer progression via microRNA-296-3p/TGIF1/TGFbeta axis.
666 *J Exp Clin Cancer Res*. 2020;39:248.
667 64. Algeciras L, Palanca A, Maestro D, RuizdelRio J and Villar AV. Epigenetic alterations of
668 TGFbeta and its main canonical signaling mediators in the context of cardiac fibrosis. *J Mol Cell*
669 *Cardiol*. 2021;159:38-47.
670 65. Nakasuka F, Tabata S, Sakamoto T, Hirayama A, Ebi H, Yamada T, Umetsu K, Ohishi M,
671 Ueno A, Goto H, Sugimoto M, Nishioka Y, Yamada Y, Tomita M, Sasaki AT, Yano S and Soga T.
672 TGF-beta-dependent reprogramming of amino acid metabolism induces epithelial-mesenchymal
673 transition in non-small cell lung cancers. *Commun Biol*. 2021;4:782.

674 66. Van Den Diepstraten C, Papay K, Bolender Z, Brown A and Pickering JG. Cloning of a
675 novel prolyl 4-hydroxylase subunit expressed in the fibrous cap of human atherosclerotic plaque.
676 *Circulation*. 2003;108:508-11.
677 67. Luo Y, Xu W, Chen H, Warburton D, Dong R, Qian B, Selman M, Gauldie J, Kolb M and
678 Shi W. A novel profibrotic mechanism mediated by TGFbeta-stimulated collagen prolyl
679 hydroxylase expression in fibrotic lung mesenchymal cells. *J Pathol*. 2015;236:384-94.
680 68. Deng B, Tang X and Wang Y. Role of microRNA-129 in cancer and non-cancerous
681 diseases (Review). *Exp Ther Med*. 2021;22:918.
682 69. Xu S, Li W, Wu J, Lu Y, Xie M, Li Y, Zou J, Zeng T and Ling H. The Role of miR-129-5p
683 in Cancer: A Novel Therapeutic Target. *Curr Mol Pharmacol*. 2022;15:647-657.
684 70. Ma R, Chen X, Ma Y, Bai G and Li DS. MiR-129-5p alleviates myocardial injury by
685 targeting suppressor of cytokine signaling 2 after ischemia/reperfusion. *Kaohsiung J Med Sci*.
686 2020;36:599-606.
687 71. Xing J, Liu J, Liu J and Xu Z. miR-129-5p ameliorates ischemia-reperfusion injury by
688 targeting HMGB1 in myocardium. *Gen Physiol Biophys*. 2020;39:461-470.
689 72. Majumdar G and Raghow R. Trichostatin A induces a unique set of microRNAs including
690 miR-129-5p that blocks cyclin-dependent kinase 6 expression and proliferation in H9c2 cardiac
691 myocytes. *Mol Cell Biochem*. 2016;415:39-49.
692
693

Figures and Figure legends

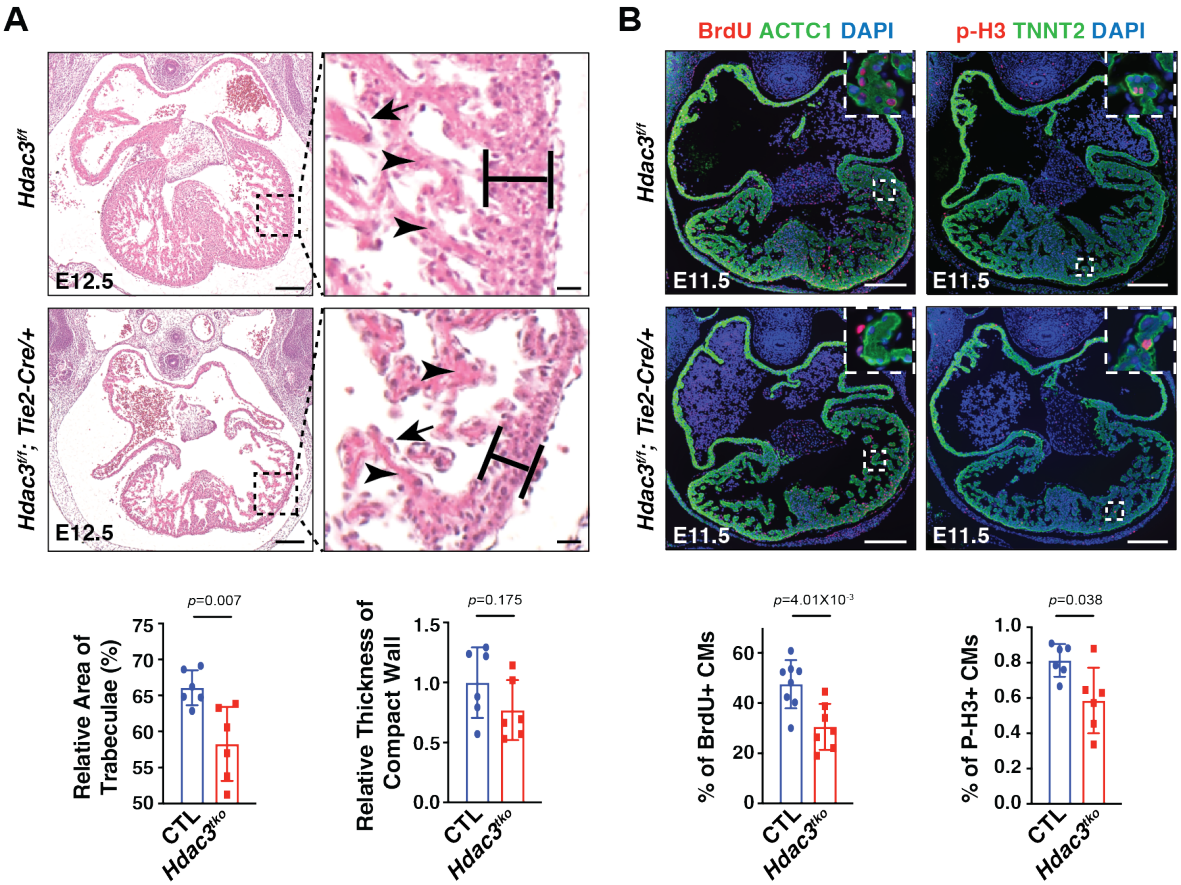

Figure 1. Endothelial specific deletion of *Hdac3* results in hypotrabeculation. **(A)** Hematoxylin and eosin staining on cross sections of an E12.5 *Hdac3*^{tko} embryo (*Hdac3*$^{f/f}$*; Tie2-Cre/*+) and a littermate control (CTL) embryo (*Hdac3*$^{f/f}$). Arrows mark endocardium and arrowheads point to trabeculae. Quantifications are shown on the bottom (n=6 in each group). Scale bars, 200 μm (main panels) and 25 μm (insets). **(B)** Decreased cardiomyocyte (CM) proliferation in E11.5 *Hdac3*^{tko} hearts. Immunofluorescence staining of Bromodeoxyuridine / 5-bromo-2'-deoxyuridine (BrdU) and phospho-Histone H3 (p-H3) staining. Scale bars, 200 μm. Quantification are shown on the bottom. BrdU (CTL: n=8, *Hdac3*^{tko}: n=7); p-H3 (n=6 in each group). *P*-values were determined by unpaired two tailed Student's *t*-test.

705

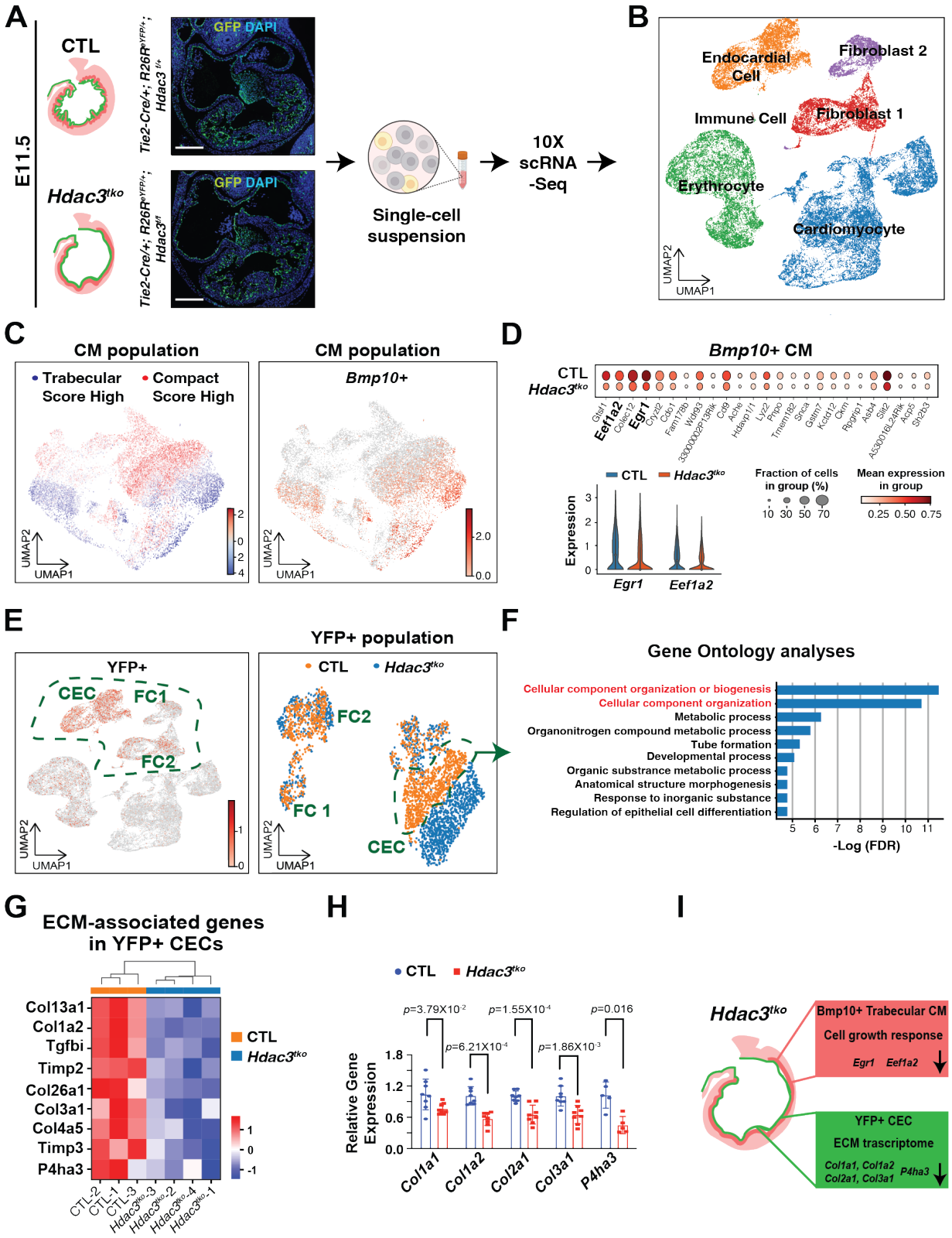

A
E11.5
CTL
Hdac3tko
Tie2-Cre/+; R26ReYFP/+; Hdac3 f/+
Tie2-Cre/+; R26ReYFP/+; Hdac3 f/f
GFP DAPI
Single-cell suspension
10X scRNA -Seq
B
Endocardial Cell
Fibroblast 2
Immune Cell
Fibroblast 1
Erythrocyte
Cardiomyocyte
UMAP2
UMAP1
C
CM population
Trabecular Score High
Compact Score High
Bmp10+
D
Bmp10+ CM
CTL
Hdac3tko
Gtsf1
Eef1a2
Colec12
Egr1
Cryzl2
Cdo1
Fam178b
Wdr93
33000002P13Rik
Cd9
Ache
Hdavp1/1
Lyz2
Pnpo
Tmem182
Snca
Gstm7
Kctd12
Ckm
Rpgrip1
Asb4
Slit2
A530016L24Rik
Acp5
Sh2b3
Fraction of cells in group (%)
10 30 50 70
Mean expression in group
0.25 0.50 0.75
Expression
Egr1
Eef1a2
E
YFP+
CEC
FC1
FC2
YFP+ population
FC 1
F
Gene Ontology analyses
Cellular component organization or biogenesis
Cellular component organization
Metabolic process
Organonitrogen compound metabolic process
Tube formation
Developmental process
Organic substrance metabolic process
Anatomical structure morphogenesis
Response to inorganic substance
Regulation of epithelial cell differentiation
-Log (FDR)
G
ECM-associated genes in YFP+ CECs
Col13a1
Col1a2
Tgfbi
Timp2
Col26a1
Col3a1
Col4a5
Timp3
P4ha3
CTL-2
CTL-1
CTL-3
Hdac3tko-3
Hdac3tko-2
Hdac3tko-4
Hdac3tko-1
H
p=3.79X10-2
p=6.21X10-4
p=1.55X10-4
p=1.86X10-3
p=0.016
Relative Gene Expression
Col1a1
Col1a2
Col2a1
Col3a1
P4ha3
I
Hdac3tko
Bmp10+ Trabecular CM
Cell growth response
Egr1 Eef1a2
YFP+ CEC
ECM trascriptome
Col1a1, Col1a2
Col2a1, Col3a1
P4ha3

706 **Figure 2. Single-cell RNA sequencing reveals decreased expression of ECM genes**
707 **in *Hdac3^{tko}* hearts.**
708 **(A)** Schematic workflow of scRNA-Seq experimental design. Representative micrographs
709 of GFP immunofluorescence staining of E11.5 *Hdac3^{tko}* embryo (*Hdac3$^{f/f}$; Tie2-Cre/+;*
710 *R26R$^{eYFP/+}$*) and a littermate control (CTL) embryo (*Hdac3$^{f/+}$; Tie2-Cre/+; R26R$^{eYFP/+}$*).
711 Scale bars, 250 μm. **(B)** UMAP visualization of cell populations in an E11.5 control heart.
712 **(C)** Trabecular and compact cardiomyocyte (CM) score were calculated within *Tnni*+ CM
713 population. Left UMAP showed CMs split into a lower cluster that has a high trabecular
714 score, and an upper cluster that has a high compact score. Right UMAP shows the
715 expression level of *Bmp10*+ per cell. **(D)** Dot plots of differentially expressed genes in
716 *Hdac3^{tko}* and CTL trabecular clusters. Violin plots of expression of *Egr1* and *Eef1a2* in
717 *Hdac3^{tko}* and CTL trabecular clusters. **(E)** The UMAP on the left shows that YFP+ cells
718 are distributed in cardiac endothelial cell (CEC, *Cdh*+), fibroblast cell 1 (FC1, *Pdgfra*+),
719 and fibroblast cell 2 (FC2, *Dcn*+) clusters. The overlapping UMAPs of *Hdac3^{tko}* and CTL
720 YFP+ cells are shown on the right. **(F)** Gene Ontology pathway analysis of top marker
721 genes in CTL-specific YFP+ CEC cluster (Cut off value: -log (FDR)>5). (**G)** Heatmap of
722 extracellular matrix (ECM) associated genes in E11.5 *Hdac3^{tko}* and CTL hearts. Data
723 were extracted from YFP+ CEC clusters in the scRNA-Seq dataset. **(H)** qRT-PCR
724 analysis of *Col1a1*, *Col1a2*, *Col2a1* and *Col3a1* and *P4ha3* in E11.5 *Hdac3^{tko}* heart as
725 compared to CTL hearts (n=8 in each group). *P*-values were determined by unpaired two
726 tailed Student's *t*-test. (**I)** Illustration of decreased expression of proliferation related
727 genes in trabecular CMs and ECM-associated genes in CECs of *Hdac3^{tko}* hearts.
728

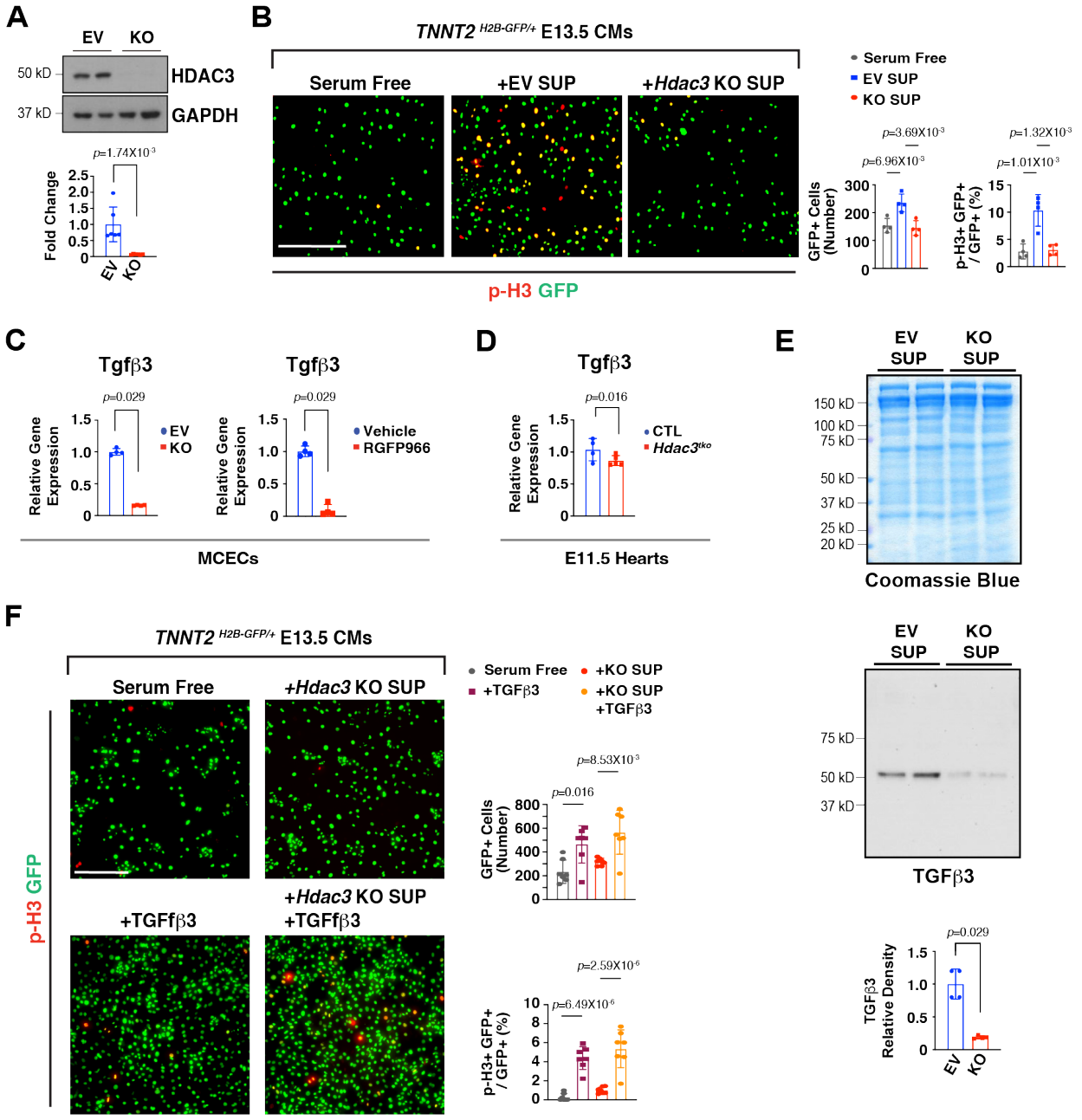

Figure 3. Cardiac endothelial *Hdac3* knockout results in downregulation of TGFβ3 and decreased cardiomyocyte proliferation.

(A) Generation of *Hdac3* knockout (KO) and empty vector control (EV) mouse cardiac endothelial cells (MCECs) by CRISPR/Cas9. Deletion of *Hdac3* was verified by western blot. Quantification is shown below (n=6 in each group). **(B)** The effects of MCEC

735 supernatants on E13.5 *Tnnt2*$^{nGFP/+}$ cardiomyocytes (CM) proliferation. Representative
736 immunofluorescence micrographs are shown. Scale bar, 275 μm. Percentage of
737 phosphor-Histone 3 (p-H3)+ CMs and total number of GFP+ CMs were quantitated (n=4
738 in each group). **(C)** Quantification of *Tgfβ3* expression in *Hdac3* KO MCECs, or
739 RGFP966-treated MCECs (10 uM) by qRT-PCR. *Gapdh* was used as cDNA loading
740 control (n=4 in each group). (**D)** Quantification of *Tgfβ3* expression in E11.5 *Hdac3*^{tko}
741 hearts by qRT-PCR. *Gapdh* was used as cDNA loading control (n=4 in each group). **(E)**
742 Secretion of TGFβ3 from *Hdac3* KO and EV MCECs. Coomassie brilliant blue staining of
743 total extracted proteins from supernatants served as protein loading controls. TGFβ3 in
744 the MCEC supernatants were detected by western blot. Quantifications are shown on the
745 right (n=4 in each group). **(F)** Rescue of CM proliferation defect by *Hdac3* KO MCECs
746 supernatant supplemented with recombinant TGFβ3 (working concentration: 250 ng/ml).
747 Representative immunofluorescence micrographs are shown. Scale bar, 200 μm.
748 Percentage of p-H3+ CMs and total number of GFP+ CMs were quantitated (n=7 in each
749 group). *P*-values were determined by unpaired two tailed Student's *t*-test for **(A)**, Mann-
750 Whitney U test for **(C)**, **(D)** and **(E)** and one-way ANOVA followed by the Tukey post hoc
751 test for **(B)** and **(F)**.
752
753

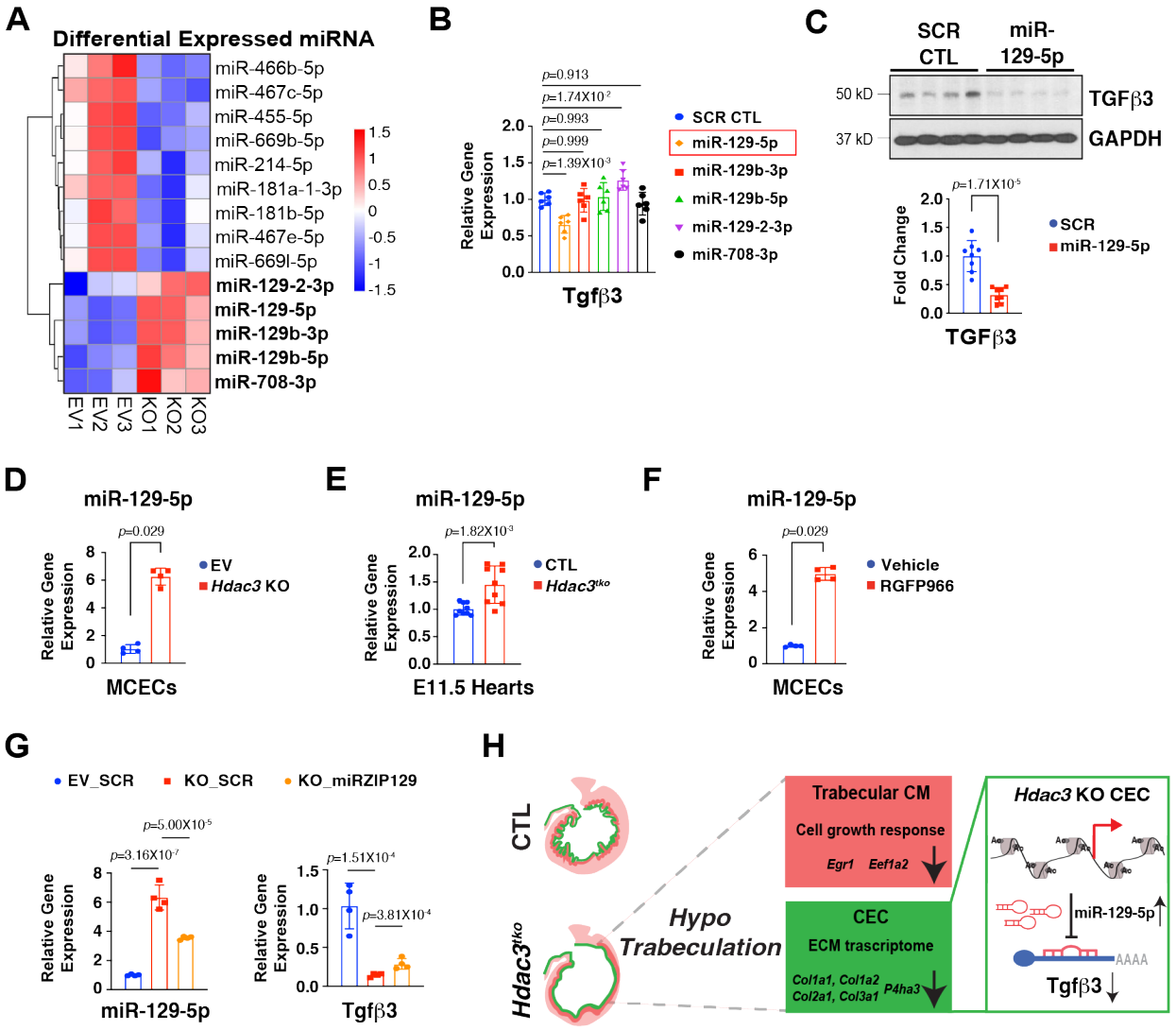

754

755 **Figure 4. HDAC3 induces Tgfβ3 by repressing miR-129-5p.**

756 **(A)** Heatmap of microRNA (miR) sequencing of *Hdac3* knockout (KO) and empty vector

757 control (EV) mouse cardiac endothelial cells (MCECs). MiRs with reads less than 100

758 were discarded and miRNA expression levels were normalized by TPM (transcript per

759 million) values (TPM = [miRNA total reads/total clean reads] × 10^6). Log_2 fold changes

760 were calculated by TPM per miR in the KO group divided by the mean TPM per miR in

761 the EV group then followed by calculation of Log (fold change, 2). Significantly

762 downregulated miRs are shown in blue, and significantly up-regulated miRs are shown in
763 red. Cut-off criteria: Log2>1.5 and adjusted *P*-value<0.01. **(B)** Quantification of *Tgfβ3*
764 expression in MCECs after miR mimics treatment (final concentration 10 nM) by qRT-
765 PCR. *Gapdh* was used as a cDNA loading control (n=6 in each group). Fold changes
766 were compared to the miR scrambles (SCR) group. **(C)** Quantification of the expression
767 of TGFβ3 after miR-129-5p mimics treatment by western blot (n=8 in each group). **(D)**
768 Quantification of the expression of *Tgfβ3* in *Hdac3* KO and EV MCECs (n=4 in each
769 group). **(E)** Quantification of the expression of *Tgfβ3* in *Hdac3*^{tko} heart lysates (n=9 in
770 each group). **(F)** Quantification of the expression of *Tgfβ3* in 10 μM RGFP966-treated
771 MCECs (n=4 in each group). **(G)** Quantification of miR-129-5p and *Tgfβ3* after *Hdac3* KO
772 or EV MECs were transfected with LentimiRa-GFP-miRZip (miR-129-5p) or pGreenPuro
773 Scramble Hairpin control lentivirus (SCR) by qRT-PCR (n=4 in each group)**.** *P*-values
774 were determined by unpaired two tailed Student's *t*-test for **(B), (C)** and **(E)**, the Mann-
775 Whitney U test for **(D)** and **(F)** and the one-way ANOVA followed by Tukey post hoc test
776 for **(G)**. **(H)** Working model: in the developing endocardium, HDAC3 represses the
777 expression of miR-129-5p to release their suppression on the expression of TGFβ3.
778 When *Hdac3* is deleted, the expression of miR-129-5p is increased, which subsequently
779 suppresses the expression of TGFβ3 to a stronger extent, and the decrease of TGFβ3,
780 together with decreased ECM, leads to hypotrabeculation.

781 **Supplemental Materials**

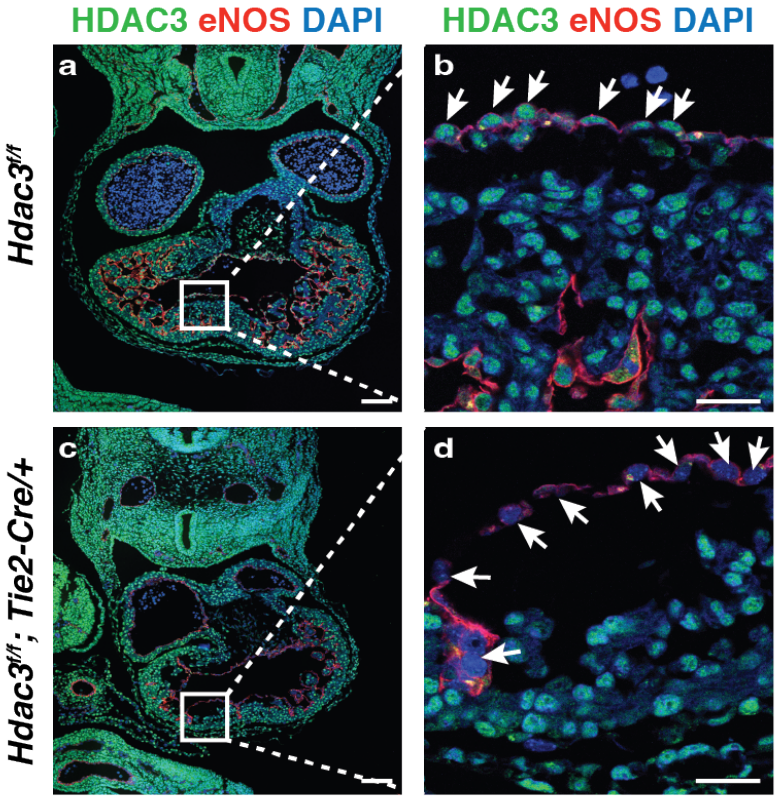

782

783 **Supplemental Figure 1. Restrictive ablation of *Hdac3* in the developing cardiac**

784 **endothelial cells.**

785 Immunofluorescence staining shows specific deletion of HDAC3 in the cardiac endothelial

786 cells (eNOS+, arrows) in E10.5 *Hdac3*^{tko} (*Hdac3*$^{f/f}$; *Tie2-Cre/*+) heart as compared to the

787 littermate control (*Hdac3*$^{f/f}$) heart (a). Scale bars, a and c, 100μm; b and d, 25 μm.

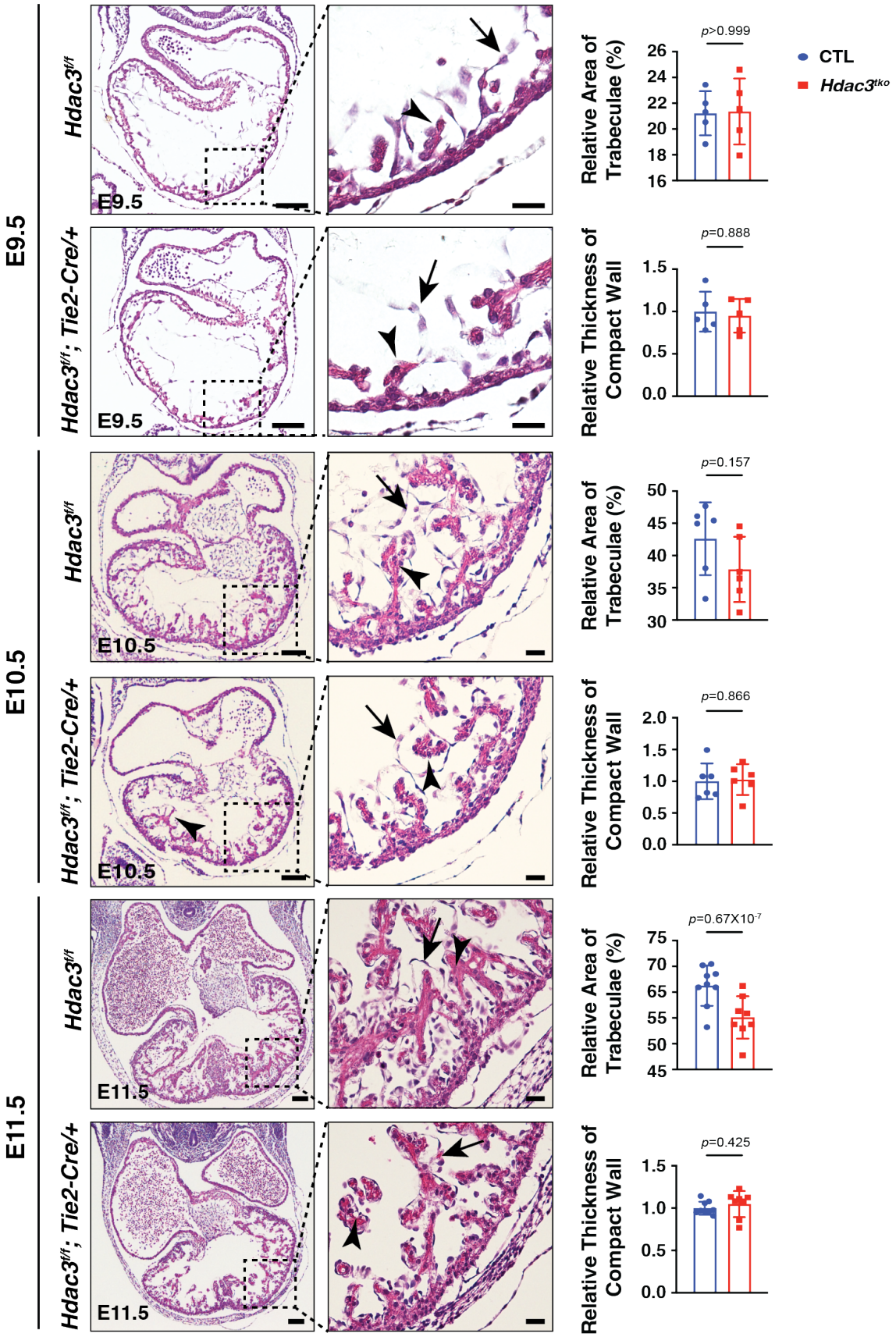
E9.5
E10.5
E11.5
Hdac3f/f
Hdac3f/f; Tie2-Cre/+
E9.5
E10.5
E11.5
Relative Area of Trabeculae (%)
Relative Thickness of Compact Wall
p>0.999
p=0.888
p=0.157
p=0.866
p=0.67X10-7
p=0.425
CTL
Hdac3tko

789 **Supplemental Figure 2. Histological analyses of cardiac phenotypes of *Hdac3^{tko}***
790 **hearts at early embryonic stages.**
791 Hematoxylin and eosin staining on cross sections of E9.5-E11.5 *Hdac3^{tko}* embryos
792 (*Hdac3$^{f/f}$; Tie2-Cre/*+) and littermate control (CTL) embryos (*Hdac3$^{f/f}$*). Arrows mark
793 endocardium and arrowheads point to trabeculae. Quantifications are shown on the right.
794 For E9.5, CTL: n=5, *Hdac3^{tko}*: n=5; For E10.5, CTL: n=6, *Hdac3^{tko}*: n=6; For E11.5, CTL:
795 n=9, *Hdac3^{tko}*: n=8. Scale bars, 100 μm and 25 μm (in insets). *P*-values were determined
796 by the Mann-Whitney U test for E9.5 embryos, and unpaired two tailed Student's *t*-test
797 for E10.5 and E11.5 embryos.

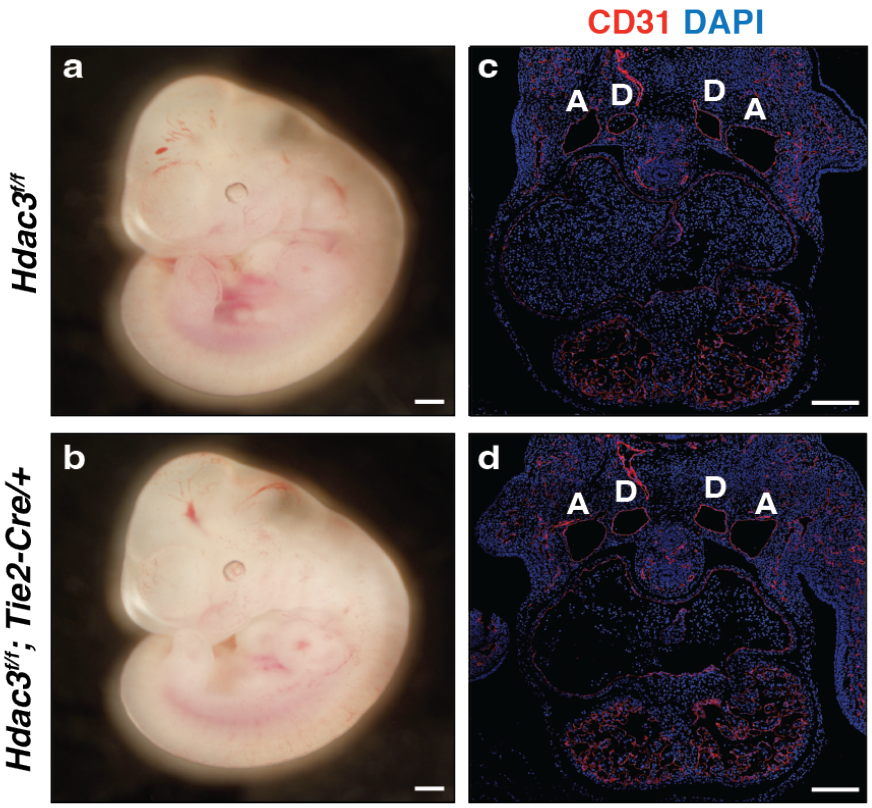

798

799 **Supplemental Figure 3. Normal vasculature in *Hdac3^{tko}* embryos.**

800 a and b, gross morphology of an E11.5 *Hdac3^{tko}* (*Hdac3$^{f/f}$; Tie2-Cre/*+) embryo (b) and an

801 E11.5 littermate control (CTL, *Hdac3$^{f/f}$*) embryo (a). b and d, immunofluorescence staining

802 of CD31. There were no apparent differences in either gross appearance or vasculature

803 between *Hdac3^{tko}* and CTL embryos. A, anterior cardinal vein; D, dorsal aorta. Scale bars,

804 a&b, 500um; c&d, 200um.

805

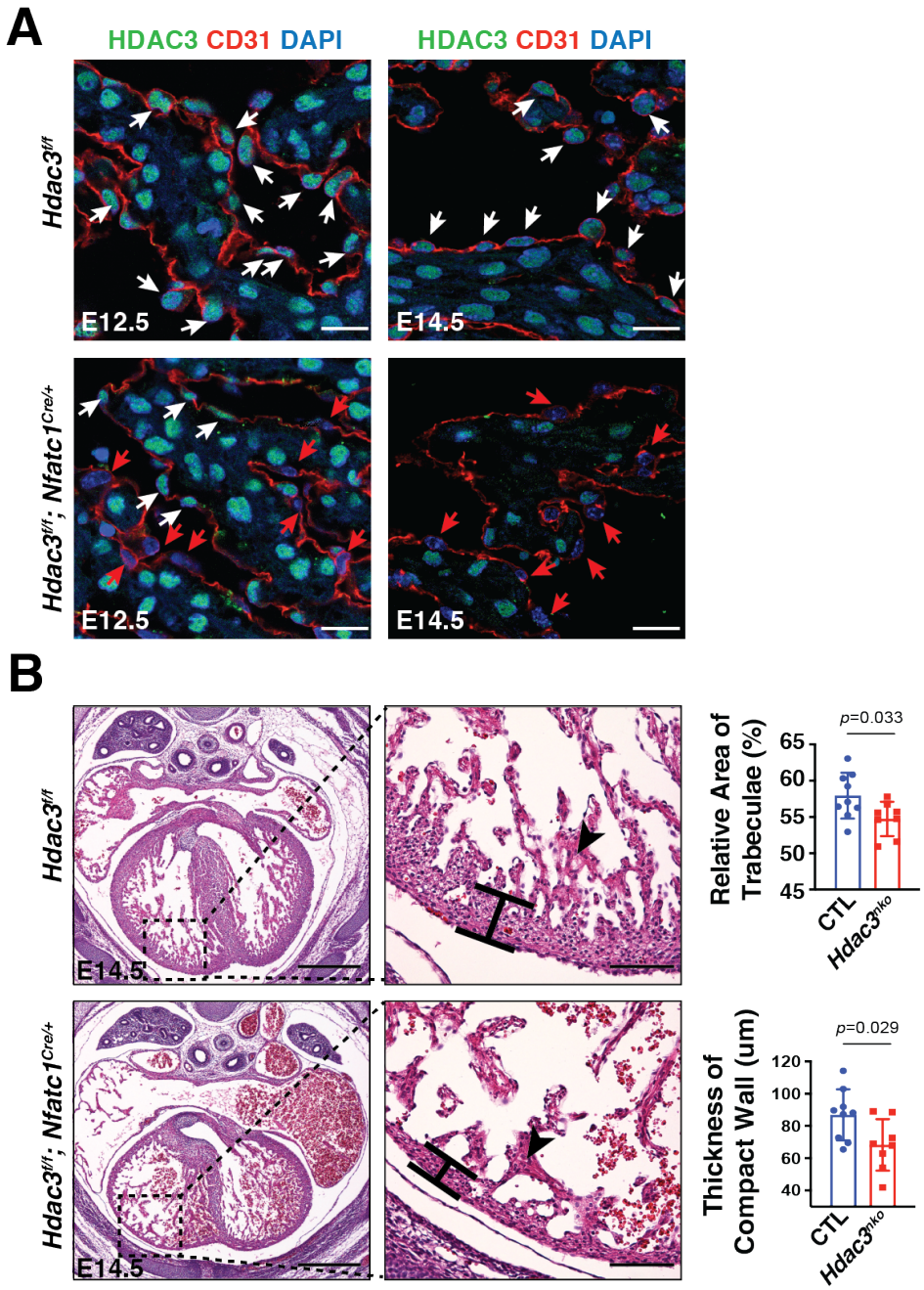

806

807 **Supplemental Figure 4. Endocardial specific deletion of *Hdac3* results in**

808 **ventricular hypoplasia.**

809 **(A)** Deletion of *Hdac3* by *Nfatc1*$^{Cre/+}$ in the developing endocardium (E12.5 and E14.5).

810 Immunofluorescence staining for HDAC3 and eNOS was performed. White arrows point

811 to endocardial cells that express HDAC3, whereas red arrows point to endocardial cells
812 in which HDAC3 is absent. Scale bars, 20 μm. **(B)** Cardiac phenotypes of E14.5 *Hdac3*
813 endocardial knockout (*Hdac3*^{nko}, *Hdac3*$^{f/f}$*; Nfatc1*$^{Cre/+}$) embryos. Arrowheads point to
814 trabeculae. Scale bars, 500 μm (main panels) and 100 μm (insets). Quantifications are
815 shown on the right. CTL: n=9, *Hdac3*^{nko}: n=8. *P*-values were determined by unpaired two
816 tailed Student's *t*-test.

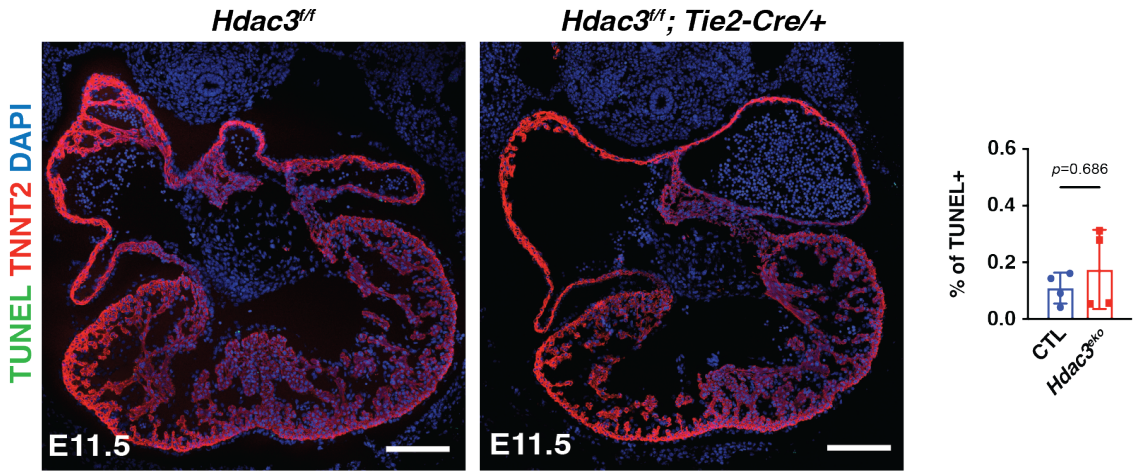

Supplemental Figure 5. Apoptosis assessment in E11.5 *Hdac3^{tko}* (*Hdac3$^{f/f}$; Tie2-Cre/+*) and littermate control (CTL, *Hdac3$^{f/f}$*) hearts by TUNEL staining. Scale bars, 100 μm. Quantitation is shown on the right (n=4 in each group). *P*-values were determined by the Mann-Whitney U test.

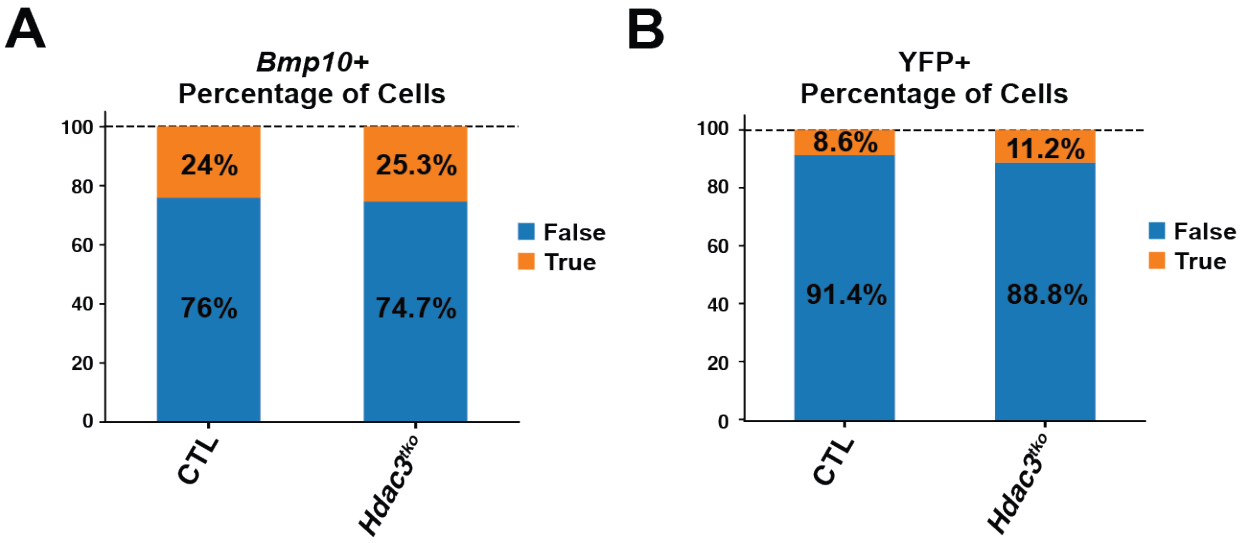

822

823 **Supplemental Figure 6. Percentage of cell number of *Bmp10+* and YFP+ cell in**

824 **E11.5 *Hdac3^{tko}* and littermate control (CTL) hearts from the scRNA-Seq dataset.**

825 **(A)** Percentage of *Bmp10* + trabecular CMs. CTL: n=4, *Hdac3^{tko}*: n=4. **(B)** Percentage of

826 YFP+ cells. CTL: n=3, *Hdac3^{tko}*: n=4.

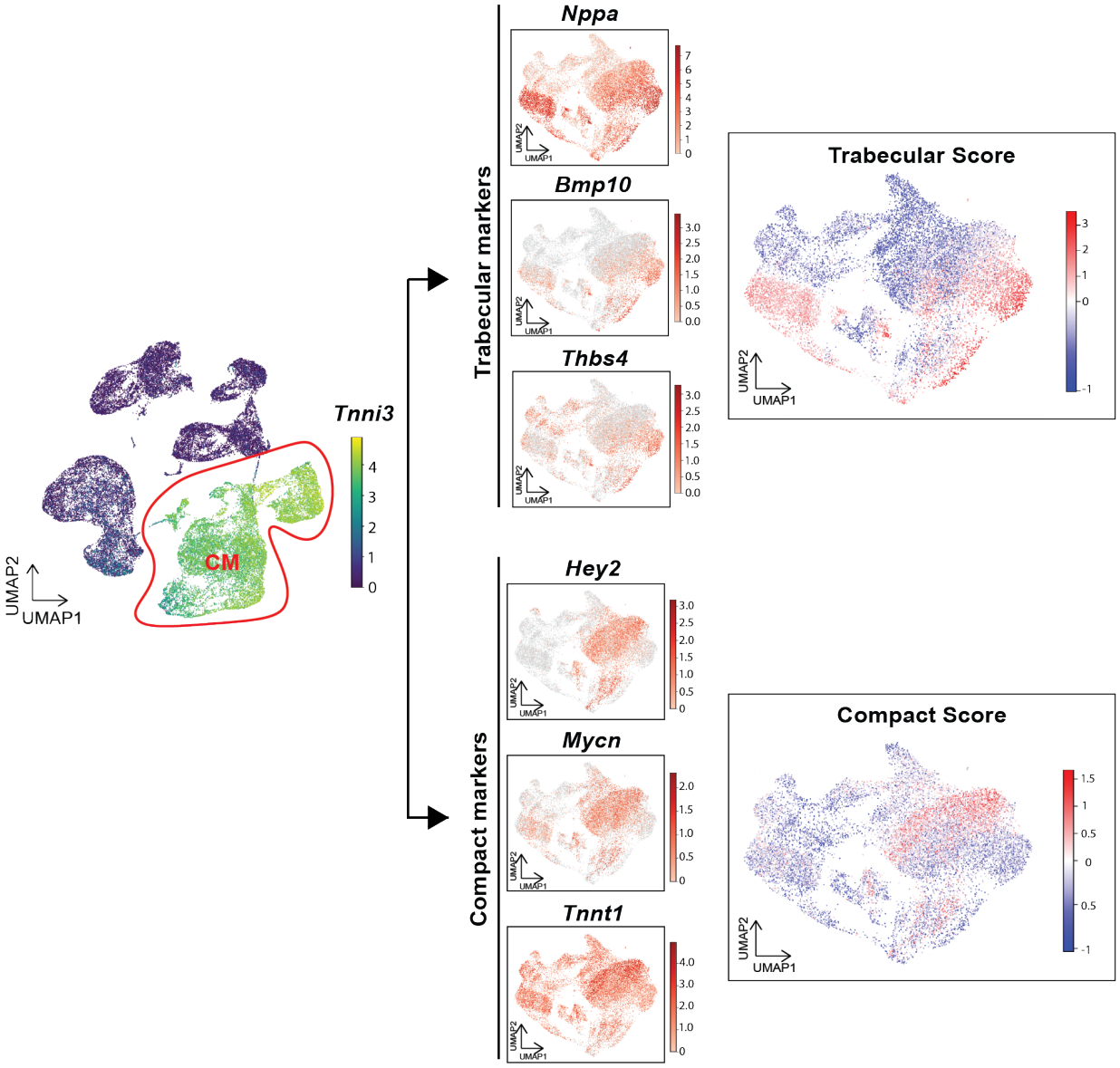

Supplemental Figure 7. UMAP plots depicting the score of trabecular and compact CMs.

Within the *Tnni3*+ E11.5 CMs, UMAP plots demonstrate the expression of trabecular CM marker genes including *Nppa*, *Bmp10* and *Thbs4*, and compact CM marker genes including *Hey2*, *Mycn* and *Tnnt1*. The calculated trabecular score and compact score are shown on the right.

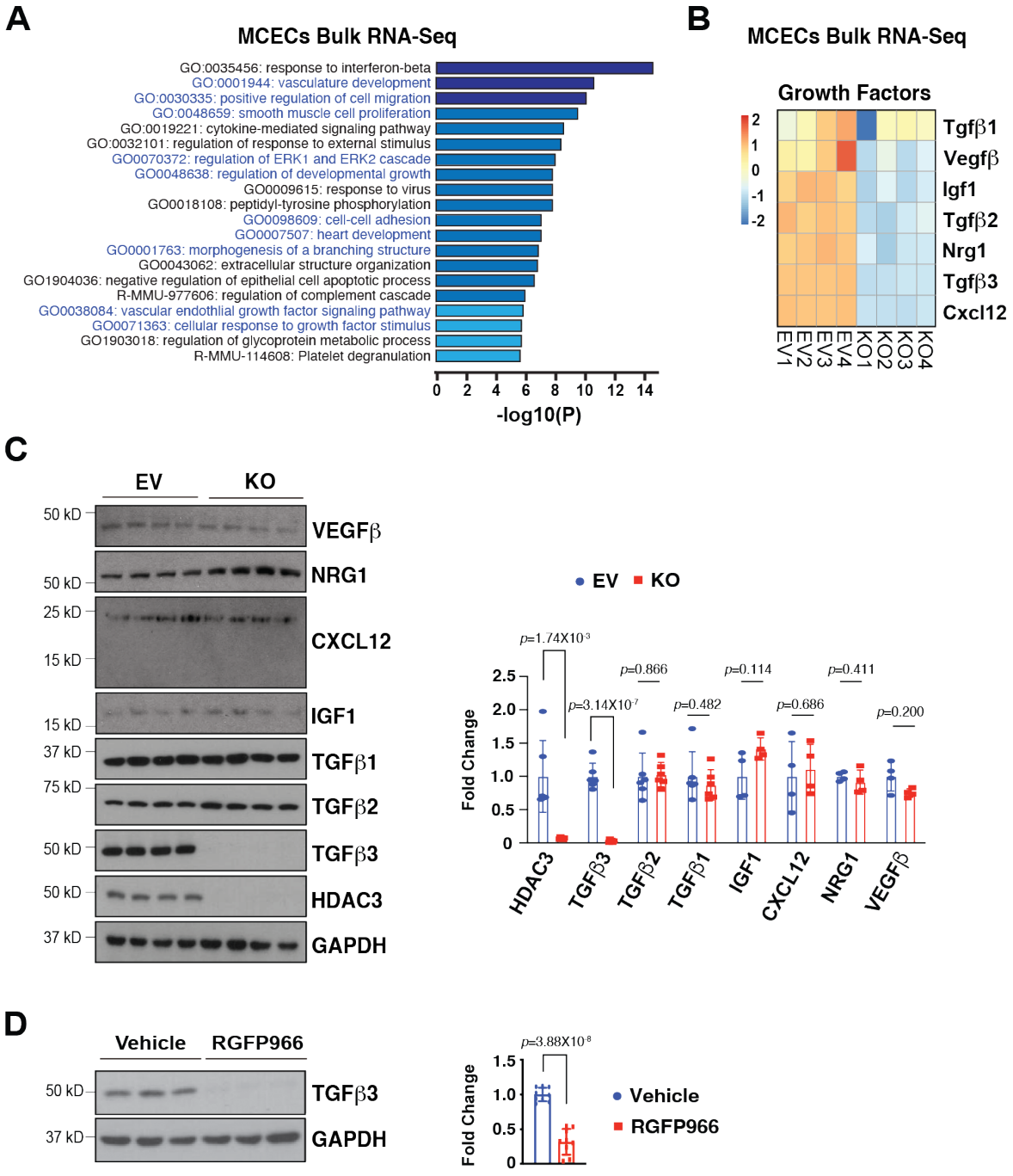

Supplemental Figure 8. HDAC3 induces the expression of Tgfß3 dependent on its deacetylase activity.

(A) Gene Ontology (GO) pathway analyses of RNA Seq in *Hdac3* KO and EV MCECs. n=4 in each group. Cut-off criteria: adjusted *P*-value<0.01. **(B)** Heatmap of growth factors

838 (*Tgfβ1*, *Vegfβ*, *Igf1*, *Tgfβ2*, *Nrg1*, *Tgfβ3* and *Cxcl12*) in in *Hdac3* KO and CTL MCECs.
839 Data were extracted from the bulk RNA-sequencing data. **(C)** Quantification of TGFβ1,
840 VEGFβ, IGF1, TGFβ2, NRG1, TGFβ3 and CXCL12 in *Hdac3* KO MCECs by western blot.
841 GAPDH was used as protein loading control. n=4 in each group. **(D)** Reduced TGFβ3
842 protein expression after RGFP966 (a selective HDAC3 inhibitor) treatment. MCEC were
843 treated with 10 uM RGFP966 or vehicle for 24 hours. n=9 in each group. *P*-values were
844 determined by the Mann-Whitney U test for **(C)** and unpaired two tailed Student's *t*-test
845 for **(D)**.

846 **Supplemental Table 1. Genotype distribution of *Hdac3^{tko}* embryos and offspring**

847 **(♂: *Hdac3$^{f/+}$; Tie2-Cre* X ♀: *Hdac3$^{f/f}$*)**

	Others (*Hdac3$^{f/f}$, Hdac3$^{f/+}$, Tie2-Cre; Hdac3$^{f/+}$*) [expected: 75%]	***Hdac3^{tko}* (*Tie2-Cre; Hdac3$^{f/f}$*) [expected: 25%]**	***p*-value**
E9.5 [n (%)]	140 (72.9%)	52 (27.1%)	0.505
E10.5 [n (%)]	168 (78.6%)	46 (21.4%)	0.2364
E11.5 [n (%)]	370 (78.6%)	101 (21.4%)	0.0747
E12.5 [n (%)]	91 (87.5%)	13 (12.5%)	0.0032*
E14.5 [n (%)]	114 (99.1%)	1 (0.9%)	<0.00001*
P0	336 (100%)	0	<0.00001*

848

849 The *p*-value was calculated by the comparison of genotype distribution and expected

850 Mendelian Ratio.

851 **Supplemental Table 2. Genotype distribution of *Hdac3^{nko}* embryos and offspring**

852 **(♂: *Hdac3$^{f/+}$; Nfatc1$^{Cre/+}$* X ♀: *Hdac3$^{f/f}$*)**

	Others (*Hdac3$^{f/f}$, Hdac3$^{f/+}$, Nfatc1$^{Cre/+}$; Hdac3$^{f/+}$*) [expected: 75%]	***Hdac3^{nko}* (*Nfatc1$^{Cre/+}$; Hdac3$^{f/f}$*) [expected: 25%]**	***p*-value**
E14.5 [n (%)]	66 (82.5%)	14 (17.5%)	0.1213
P0	209 (100%)	0	<0.00001*

853

854 The *p*-value was calculated by the comparison of genotype distribution and expected

855 Mendelian Ratio.